Review Article

Qipeng Zhang, Jiayi Xu, Chaoyue Li, Jiguang Dong, Yong Wang, Chenglong Shi*, and Yaru Qin*

Research progress on rubidium and cesium separation and extraction

https://doi.org/10.1515/rams-2025-0139
received February 15, 2025; accepted July 18, 2025

Abstract: Rubidium (Rb) and cesium (Cs), as rare alkali metals, exhibit wide application potential in fields such as medicine, laser materials, catalysts, and aerospace due to their unique physicochemical properties. In recent years, with the continuous growth in the demand for rubidium and cesium, efficient separation techniques for these elements have gradually become a hot research topic. This review systematically summarizes the latest research progress on major rubidium and cesium separation techniques, including precipitation, solvent extraction, membrane separation, and adsorption methods. The characteristics and applicability of each technique are discussed, and the future development directions of rubidium and cesium separation and extraction technologies, along with their prospects in practical applications, are envisioned.

Keywords: rubidium, cesium, separation and extraction

*** Corresponding author: Chenglong Shi**, School of Chemistry and Materials Science, Qinghai Minzu University, 810007, Xining, China; Qinghai Provincial Key Laboratory of Nanomaterials and Technology, Qinghai Minzu University, 810007, Xining, China, e-mail: shiclong@qhmu.edu.cn
*** Corresponding author: Yaru Qin**, School of Chemistry and Materials Science, Qinghai Minzu University, 810007, Xining, China; Qinghai Provincial Key Laboratory of Nanomaterials and Technology, Qinghai Minzu University, 810007, Xining, China, e-mail: yaruqin@qhmu.edu.cn
Qipeng Zhang, Jiayi Xu, Chaoyue Li: School of Chemistry and Materials Science, Qinghai Minzu University, 810007, Xining, China; Qinghai Provincial Key Laboratory of Nanomaterials and Technology, Qinghai Minzu University, 810007, Xining, China
Jiguang Dong: School of Chemistry and Materials Science, Qinghai Minzu University, 810007, Xining, China; Key Laboratory of Comprehensive and Highly Efficient Utilization of Salt Lake Resources, Qinghai Institute of Salt Lakes, Chinese Academy of Sciences, 810008, Xining, China
Yong Wang: School of Chemistry and Materials Science, Qinghai Minzu University, 810007, Xining, China

1 Introduction

Rubidium (Rb) and cesium (Cs) are rare alkali metals located in Group I of the periodic table, with unique physical, chemical, and optoelectronic properties. Rubidium, cesium, and their compounds exhibit significant application potential in various fields, including atomic clocks [1], aerospace [2], specialty glasses [3,4], catalysts [5], perovskite solar cells [6], medicine [7], sensors [8], and optoelectronic materials [9]. As a result, these elements have attracted considerable attention. With the rapid advancement of technology, the demand for rubidium and cesium has been continuously increasing. However, the process of extracting rubidium and cesium from minerals is complex and technologically challenging, leading to limited production and high prices. In nature, rubidium and cesium generally occur together due to their similar chemical properties, making their separation difficult. Independent rubidium and cesium minerals are extremely rare and are usually found in association with other rare metals such as lithium, beryllium, tantalum, and niobium in granitic pegmatites, salt lake brines, or seawater [10]. The concentrations of Rb^+ and Cs^+ in salt lake brines and seawater are very low, existing only in trace or ultratrace amounts, and are accompanied by high concentrations of Na^+ and K^+, resulting in low-grade resources.

Globally, the reserves of rubidium in granite pegmatites and cesium in pollucite are concentrated primarily within three countries: Zimbabwe, Namibia, and Canada. The estimated reserves of Rb_2O in foreign granite pegmatites are approximately 1.7×10^5 t, with the three countries above accounting for 1.62×10^5 t, representing 95% of the foreign rubidium resources. The distribution of these reserves is illustrated in Figure 1. The total reserves of Cs_2O in foreign countries amount to 2.171×10^5 t, with these three nations collectively holding 64% of the world's cesium ore reserves. Additionally, substantial amounts of rubidium and cesium resources are present in salt lake brines both domestically and internationally. For instance, the Salton Sea in the United States contains rubidium and cesium concentrations of 169 and 20 $mg \cdot L^{-1}$, respectively.

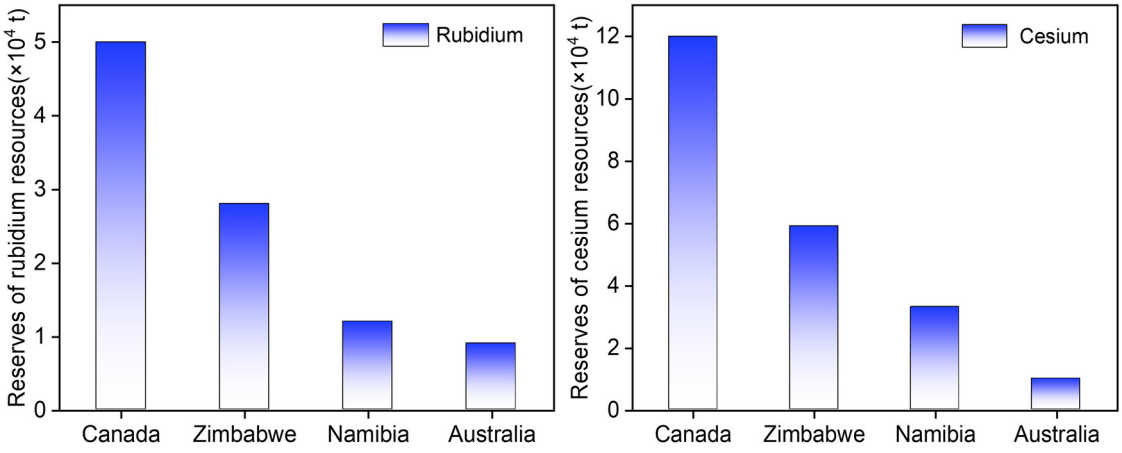

Figure 1: Distribution diagram of rubidium and cesium resources [11].

The rubidium and cesium concentrations in global natural salt lake brines are detailed in Table 1.

China is rich in rubidium and cesium resources, primarily distributed in the form of ions in salt lake brines, with some existing as solid minerals in pollucite and lepidolite. Salt lake resources in China are widely distributed in regions such as Qinghai and Tibet, covering a total area of 37,927 km^2, including 37 surface salt lakes and 7 dry salt lakes [12]. Although the concentrations of rubidium and cesium in salt lake brines are low, the total resource amount is abundant, providing significant potential for industrial development. However, existing rubidium and cesium mineral resources can no longer meet the rapidly growing industrial demand, making the extraction of rubidium and cesium from salt lake brines increasingly important. In salt lake brines, rubidium and cesium coexist with alkali metal ions such as Li^+, Na^+, and K^+, particularly as the ionic radius of K^+ is close to that of Rb^+ and Cs^+, which significantly increases the separation difficulty and represents a major technical bottleneck in current rubidium and cesium extraction processes. Therefore, reducing the extraction cost and energy consumption and simplifying the extraction process are key directions for future research and application. This article reviews recent research progress on rubidium and cesium separation and extraction technologies, systematically analyzes the advantages and disadvantages of various separation techniques, and, based on the current research status, envisions the future technological development directions for achieving stable and efficient rubidium and cesium separation.

Table 1: Natural salt lakes containing Rb^+ and Cs^+ worldwide [12]

Country	Area	Rb^+ ($mg \cdot L^{-1}$)	Cs^+ ($mg \cdot L^{-1}$)
Russia	Siberian salt lake	21	—
Russia	Ur dry lake	0.3–20	—
Israel	Dead sea	60	—
USA	Salton salt lake	137–169	16–20
USA	Wood salt lake	25	25
China	Qarhan salt lake	10.8–14	0.034
China	Zabuye salt lake	50–60	12–21
China	Weiyuan gas field	5.2	11.9
Japan	Arima onsen	3.5	3.5

2 Rubidium and cesium separation methods

Rubidium and cesium resources in China are primarily found in salt lake brines. Efficiently separating rubidium and cesium from solutions has become a current research focus. Existing methods for the separation and extraction of rubidium and cesium mainly include precipitation, solvent extraction, membrane separation, and adsorption.

2.1 Precipitation method

The precipitation method is a commonly used technique for separation and purification, which involves adjusting the chemical reaction conditions (such as reaction time, temperature, pH, *etc.*) to form insoluble precipitates of the target substances in the solution. Common precipitating agents for rubidium and cesium include complex salts, polyhalides, heteropoly acids, and alum compounds, among which sodium tetraphenylborate (NaTPB), phosphotungstic acid, and potassium bismuth iodate have

been widely studied. For example, Fang *et al.* [13] successfully extracted Rb^+ and Cs^+ from aqueous solutions using a precipitation flotation method. As shown in Figure 2, when ammonium phosphotungstate (AWP) is used as the precipitating agent, cetyltrimethylammonium bromide (CTAB) as the collector and frother, and the reaction conditions are set with a pH of 10, a CTAB concentration of 0.15 mmol·L^{-1}, Rb^+/Cs^+ concentration of 1 mmol·L^{-1}, and a molar ratio of AWP to Rb^+/Cs^+ of 1:1, the extraction efficiency of rubidium and cesium approaches 100% and Rb^+ and Cs^+ precipitated as $Rb_3PWO_{12}O_{40}{\cdot}xH_2O$ and $Cs_3PWO_{12}O_{40}{\cdot}xH_2O$.

Li *et al.* [14] employed the $Cs_3Bi_2I_9$ precipitation method to efficiently separate cesium (Cs^+) from a solution containing both Rb^+ and Cs^+, achieving an impressive Cs^+ recovery rate of 98.55%. In this process, cesium ions are selectively precipitated as $Cs_3Bi_2I_9$. Following vacuum thermal decomposition, $Cs_3Bi_2I_9$ is transformed into cesium iodide (CsI) and bismuth iodide (BiI_3). The resulting CsI products demonstrate a purity greater than 99%. This method offers several key advantages, including low operational costs, minimal processing time, environmental sustainability, and ease of operation.

Soliman *et al.* [15] studied the isotope dilution precipitation flotation method for removing ^{137}Cs from low-level radioactive wastewater. In this method, NaTPB is used as the precipitant, and sodium lauryl sulfate and cetylpyridinium chloride surfactants serve as collectors, effectively extending the pH applicability range of the flotation process. In the presence of Fe(III), an iron oxide coating can form, effectively precipitating ^{137}Cs. Lu *et al.* [16] investigated the hydrometallurgical process for extracting Cs^+ from the Taron deposit in Argentina, using sulfuric acid leaching and sulfuric acid with sulfur dioxide reduction leaching. The Cs^+ in the leachate was finally precipitated in the form of cesium alum. In the next phase, the pure cesium alum was dissolved in hot water, and the resulting solution was subjected to a two-step treatment with barium hydroxide, as depicted in Figure 3. In the first step, aluminum hydroxide and part of the barium

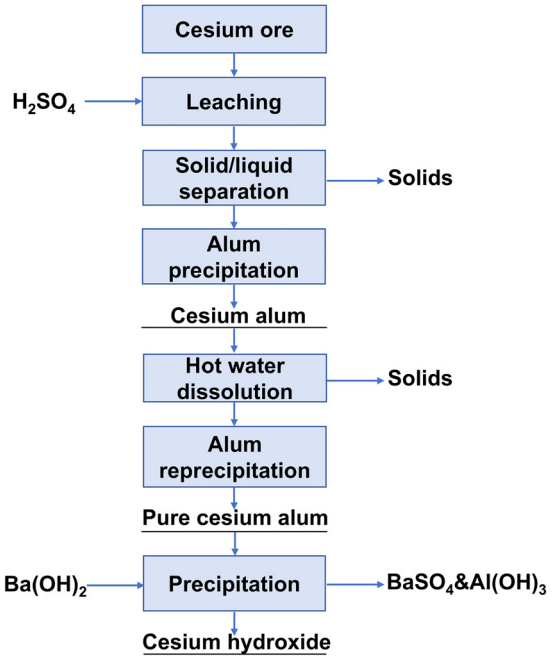

Figure 3: Cesium alum recovery process of cesium [16].

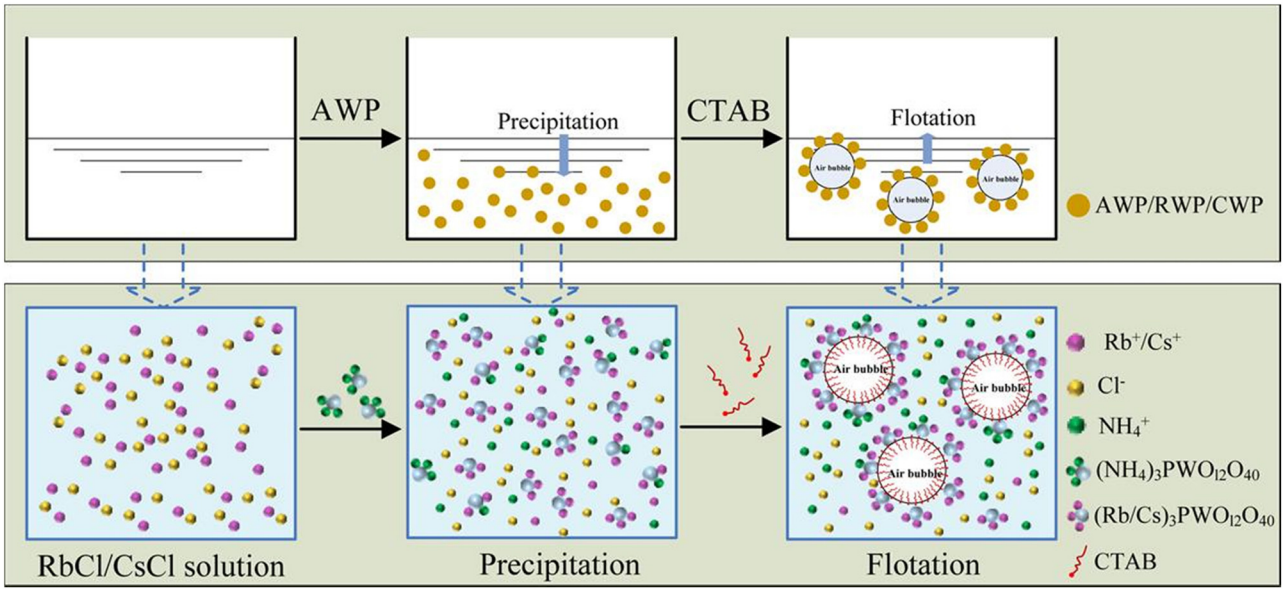

Figure 2: Technical route of AWP precipitation method [13].

sulfate were removed from the solution. The remaining barium sulfate and other impurities were then eliminated in the second step. This dual-stage process ensured the efficient removal of contaminants and facilitated the isolation of cesium hydroxide, which remained in the final solution. The cesium hydroxide obtained can then be converted into various cesium salts through the addition of appropriate acids, enabling the production of different cesium-based products.

Table 2 lists the literature reported in recent years on the separation of rubidium and cesium using the precipitation method. Although the precipitation method can efficiently extract Rb^+ and Cs^+, its practical application remains limited. This technology was widely used in early industrial production, primarily for processing high-concentration Rb^+ and Cs^+ aqueous solutions. However, in salt lake brine and seawater, the concentrations of these two ions are generally low. Additionally, the precipitation method involves a complex process, is more costly, and the resulting precipitates often exhibit poor stability and low purity. Therefore, there has been relatively little research on the use of the precipitation method to extract Rb^+ and Cs^+ from low-concentration solutions.

2.2 Solvent extraction method

The solvent extraction method is a separation and enrichment technique based on the differences in solubility or partition coefficients of compounds between two immiscible solvents. By transferring target compounds from one solvent to another, this method achieves selective separation. In recent years, solvent extraction has been widely applied in rubidium and cesium separation studies and has gained attention due to its rapid reaction kinetics, high efficiency, and operational simplicity. Commonly used extractants for rubidium and cesium include crown ethers, phenolic alcohols, dipicrylamine, and nitro compounds. However, research on dipicrylamine and nitro compounds as extractants remains relatively scarce due to their high toxicity and the difficulty of stripping.

2.2.1 Crown ether extractants

The binding affinity of crown ethers is closely related to the size and shape of the target ion, and thus they can be used to selectively recognize and bind specific metal ions. The complexation behavior of crown ethers with alkali metal ions arises from a combination of noncovalent interactions, including ligand coordination, cation–π interactions, CH–π interactions, and both C–H and O–H hydrogen bonds. The incorporation of a cuproaromatic moiety significantly enhances the stability of the resulting complexes [24]. For example, Wang *et al.* [25] investigated the complexation mechanisms of crown ether derivatives (18C6, 21C7, B18C6, B21C7) with alkali metal ions (Li^+, K^+, Rb^+, Cs^+). Their study revealed that interactions between alkali metal ions and oxygen atoms in crown ether molecules elongate C–O bonds after complexation, primarily driven by electrostatic attraction. The introduction of benzene ring substituents enhances the electrophilic substitution activity of crown ethers but reduces their electrophilic complexation reactivity. He *et al.* [26] employed diaminobenzo-18-crown-6 (DAB18C6) as the extractant and $[C_4mim][PF_6]$, $[C_6mim][PF_6]$, and $[C_4mim][NTf_2]$ as co-extractants. Results demonstrated that the Cs^+ extraction efficiency in the DAB18C6-$[C_4mim][NTf_2]$ liquid–liquid system reached 99.94% under optimized conditions, exhibiting high selectivity for Cs^+. The extraction mechanism involves a cation exchange reaction between Cs^+ and $[C_4mim]^+$, while $[NTf_2]^-$ coordinates with DAB18C6-Cs^+ to form a stable ternary complex, DAB18C6-$Cs^+[NTf_2]^-$.

2.2.2 Phenolic alcohol extractants

Among phenolic alcohol reagents, 4-sec-butyl-2-(α-methylbenzyl) phenol (BAMBP) and 4-tert-butyl-2-(α-methylbenzyl)phenol

Table 2: Comparison of the precipitation performance of different precipitants

Precipitant	Condition	Sedimentation rate (%)	Ref.
$K_4[Fe(CN)_6]/FeSO_4/Ni(NO_3)_2$	c_{Cs^+} = 0.1 mol·L^{-1}, pH = 9.5	99.91	[17]
$Ni(NO_3)_2/K_4Fe(CN)_6$	c_{Cs^+} = 1 mg·L^{-1}, pH = 7, T = 25°C	94.53	[18]
CuHCF	c_{Rb^+} = 6.99 g·L^{-1} C_{Cs^+} = 8.59 g·L^{-1}, T = 25°C, t = 10 min	Rb^+: 88.84, Cs^+: 99.78	[19]
Zeolite/$BaSO_4$	c_{Cs^+} = 25 ppm, T = 25°C, t = 40 min	98	[20]
Zeolite/$BaSO_4$	c_{Cs^+} = 25 ppm, t = 15 min	95.7	[21]
$Al_2(SO_4)_3$	c_{Rb^+} = 13.83 g·L^{-1}, pH = 6.02	95	[22]
$Mg_3Si_2O_5(OH)_4/H_3PO_4$	c_{Cs^+} = 1 mmol·L^{-1}, t = 3 h, T = 25°C	95	[23]

(t-BAMBP) are the commonly used extractants, exhibiting extraction selectivity in the order $Cs^+ > Rb^+ > K^+ > Na^+ > Li^+$. However, BAMBP is less practical for industrial applications due to its low extraction efficiency and high cost. In contrast, t-BAMBP, as its isomer, offers advantages such as higher extraction efficiency, shorter extraction time, ease of back-extraction, excellent recyclability, and cost-effectiveness, making it widely applicable in rubidium and cesium extraction [27]. Chen *et al.* [28] developed a process involving the selective removal of K^+ by perchloric acid precipitation, followed by solvent extraction and back-extraction of Rb^+ and Cs^+ from concentrated seawater using t-BAMBP and ammonia-mediated stripping. Under optimized conditions, the extraction and back-extraction efficiencies reached 99.8 and 99.9% for Cs^+, and approximately 98.3 and 95% for Rb^+, respectively. Aqueous solutions of rubidium hydroxide and cesium hydroxide were obtained following back-extraction. These were subsequently reacted with ammonium carbonate to yield rubidium carbonate and cesium carbonate. A schematic diagram of the process is shown in Figure 4.

The t-BAMBP molecule forms cage-like ionic complexes with Cs^+ and Rb^+, thereby reducing the polarity of the ionophore and enhancing its solubility in the organic phase. Simultaneously, cation–π interactions between Cs^+ and Rb^+ and the π–electron cloud of the benzene ring in t-BAMBP further stabilize the ionophore complex. During the stripping process, protons under acidic conditions replace Cs^+ and Rb^+ in the complex, regenerating the phenolic hydroxyl groups in the t-BAMBP molecule. For example, Xie *et al.* [29] utilized t-BAMBP to separate Rb^+ and Cs^+ from solutions containing high concentrations of K^+ and Na^+. After five-stage countercurrent extraction, Rb^+ and Cs^+ extraction efficiencies reached 99.81 and 98.09%, respectively, with a K^+ co-extraction rate of 19.31. Following five-stage countercurrent washing with deionized water (O/A ratio 2:1) approximately 99.32% of K^+ was removed from the organic phase. Using 0.5 $mol \cdot L^{-1}$ HCl as the washing agent under an O/A ratio of 3:1 in two-stage countercurrent washing, nearly all Rb^+ and Cs^+ (>99%) were recovered. The extraction mechanism of t-BAMBP, a weakly acidic extractant, involves ion exchange between the hydrogen atom of the phenolic hydroxyl group and alkali metal ions. Lv *et al.* [30,31] investigated the selective extraction of Cs^+ from lepidolite leachate using t-BAMBP as the extractant and xylene as the diluent. Under optimized conditions, Cs^+ extraction efficiency reached 99.18%. Slope analysis and infrared spectroscopy confirmed that the extraction proceeds *via* an ion exchange mechanism between t-BAMBP and Cs^+. The team further developed a protocol for Rb^+ extraction from impurity-rich solutions, systematically evaluating factors such as contact time, extractant concentration, alkalinity, and phase ratio. Four-stage countercurrent extraction under optimized conditions yielded 99.07% Rb^+ extraction efficiency. After washing the loaded organic phase with deionized water to remove impurities, rubidium salts with a purity of 99.5% were obtained. In an innovative approach, Chen and Hu [32] introduced a crystal ripening microextraction technique for direct Rb^+ recovery from solid KCl salts (Figure 5). Utilizing t-BAMBP as the extractant and sulfonated kerosene as the dispersant, this method leverages induced lattice restructuring to achieve *in situ* Rb^+ extraction. Compared to conventional liquid–liquid extraction, this approach demonstrated superior extraction efficiency, separation factors, and energy efficiency, with broad applicability for target metal recovery from diverse solid metal salts.

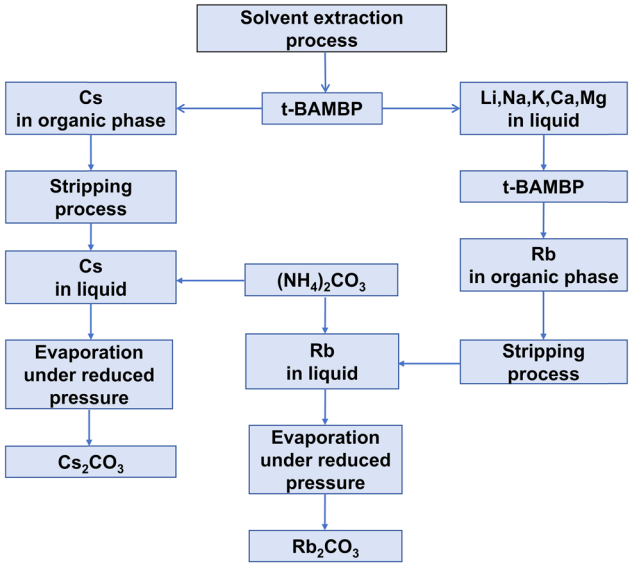

Figure 4: Process for the preparation of pure rubidium and cesium salts from seawater [28].

Solvent extraction is widely employed for the separation of rubidium and cesium owing to its operational simplicity, fast kinetics, and high efficiency. However, synthesizing highly selective extractants is often technically demanding and costly, and the organic diluents routinely used are often toxic. Moreover, the process is susceptible to emulsification, which limits repeated extraction–stripping cycles. Despite these drawbacks, solvent extraction remains highly promising because of its exceptional selectivity toward Rb^+ and Cs^+. Table 3 summarizes recent reports on rubidium and cesium separation *via* solvent extraction techniques.

2.3 Membrane separation method

The membrane separation method is a technique that achieves component separation in solutions through the

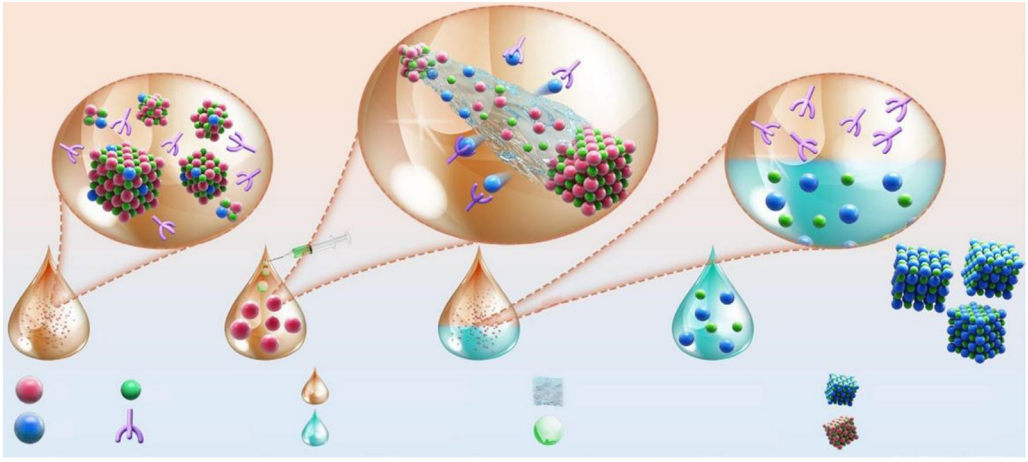

Figure 5: Schematic diagram of the crystal ripening microextraction strategy for rubidium recovery from solid potassium chloride salts [32].

selective permeability of semipermeable membranes. This method is widely applied in water treatment, food processing, and biomedicine. Membrane separation processes typically operate under low pressure, offering lower energy consumption compared to conventional high-energy-consumption separation methods. By selecting membranes with different pore sizes and properties, effective separation of substances with varying molecular weights can be achieved.

Shi *et al.* [40] developed a novel polymeric nanofiber membrane *via* electrospinning for efficient and selective Rb^+ capture from hypersaline solutions. Their findings revealed that increasing the phenolic hydroxyl group density on the membrane surface enhanced Rb^+ adsorption capacity to 53.15 $mg{\cdot}g^{-1}$. Remarkably, the membrane maintained over 85% recovery after five adsorption–desorption cycles, demonstrating significant potential for rubidium separation and purification. Sun *et al.* [41] immobilized AWP on polysulfone porous membranes using NIPs technology to fabricate mixed matrix membranes. Experimental results indicated that higher phosphotungstate content improved membrane hydrophilicity and flux. Under optimal conditions, the membrane achieved an Rb^+ adsorption capacity of 98.4 $mg{\cdot}g^{-1}$, with recovery rates exceeding 95% after five cycles. Jia *et al.* [42] engineered Prussian blue (PB) and polydopamine (PDA) composite layers on porous polyacrylonitrile (PAN) membranes for radioactive Cs^+ adsorption. First, *in situ* polymerization of dopamine on PAN membranes yielded PDA/PAN membranes with a Cs^+ adsorption capacity of 0.074 $mmol{\cdot}g^{-1}$. Subsequent PB layer deposition on PDA/PAN significantly enhanced adsorption capacity to 0.498 $mmol{\cdot}g^{-1}$. Liu *et al.* [43] synthesized quaternary ammonium-functionalized aldehyde monomer (HBAB)-C_3-symmetric 2,4,6-tri(4-aminophenyl)-1,3,5-triazine (TAPA)-covalent organic framework (COF) multilayer membranes on PAN substrates (synthetic route shown in Figure 6) using HBAB and TAPA. The optimized membrane exhibited a Cs^+ permeability of 0.33 $mol{\cdot}m^{-2}{\cdot}h^{-1}$ and an exceptional Cs^+/La^{3+} separation factor of 75.9 in single-ion systems, highlighting its promise for rare

Table 3: Recent advances in solvent-extraction-based separation of rubidium and cesium

Extractants	Solvent	*E* (%)	*β* or *D*	Ref.
Calix[4]arene crown-6	1,2-Dichloroethane	—	D_{Cs} = 0.116	[33]
t-BAMBP	Sulfonated kerosene	98.60	$\beta_{Cs/K}$ = 120.30 $\beta_{Cs/Rb}$ = 56.90	[34]
t-BAMBP	Sulfonated kerosene	99.2	$\beta_{Cs/Rb}$ = 24.06	[35]
t-BAMBP	Sulfonated kerosene	99.10	$\beta_{Cs/K}$ = 1550.70 $\beta_{Cs/Rb}$ = 45.20	[36]
t-BAMBP	ShellSol D70	>99	$\beta_{Cs/K}$ = 135 $\beta_{Cs/Rb}$ = 11	[37]
DCH18C6	C_2mim][NTf_2]/1,2-dichloroethane	93.63	—	[38]
t-BAMBP	Kerosene	Rb^+: 95.04 Cs^+: 99.80	—	[39]

metal ion separation. Jia *et al.* [44] immersed a PAN membrane into potassium ferrocyanide and ferric chloride solutions to form a uniform and robust iron ferrocyanide nanolayer on the membrane surface. This membrane exhibited high adsorption capacity and selectivity for cesium, along with excellent desorption and regeneration performance. He *et al.* [45] prepared a novel polyimide porous membrane (PI-18C6) by covalently grafting dibenzo-18-crown-6 (DB18C6) functional groups onto a polyimide backbone. The membrane achieved a Cs^+ adsorption capacity of 54.08 $mg \cdot g^{-1}$ and demonstrated strong selectivity against coexisting ions such as K^+, Na^+, Mg^{2+}, and Rb^+. Theoretical calculations revealed that the adsorption energy of PI-18C6 for Cs^+ was higher than that for K^+ and Rb^+ (Figure 7), attributed to the match between the inner diameter of DB18C6 and the ionic diameter of Cs^+, which significantly enhanced Cs^+ adsorption. Zhang *et al.* [46] developed a cesium ion-imprinted composite membrane (I-DBC) for selective Cs^+ separation using bacterial cellulose as a carrier, combined with hydrophilic dopamine-mimetic bonding and ion imprinting technology. The I-DBC membrane exhibited a maximum adsorption capacity of 50.016 $mg \cdot g^{-1}$ and a capacity of 4.03 $mg \cdot g^{-1}$ in low-concentration wastewater, alongside excellent permeability, highlighting its potential for nuclear wastewater treatment.

Membrane separation combines energy efficiency, operational simplicity, and high selectivity, but several practical obstacles constrain its wider deployment. Membrane fouling progressively diminishes flux and selectivity, necessitating routine cleaning or periodic membrane replacement. Prolonged operation can also induce material ageing and mechanical degradation, shortening service life. In addition, concentration polarization that develops during enrichment steps further erodes separation performance. Nevertheless, the technique remains an energy-efficient and environmentally benign option with considerable scope for future advancement.

2.4 Adsorption method

The adsorption method is primarily used to concentrate, separate, and extract Rb^+ and Cs^+ from low-concentration solutions. It is regarded as one of the most promising technologies due to its high exchange capacity, excellent

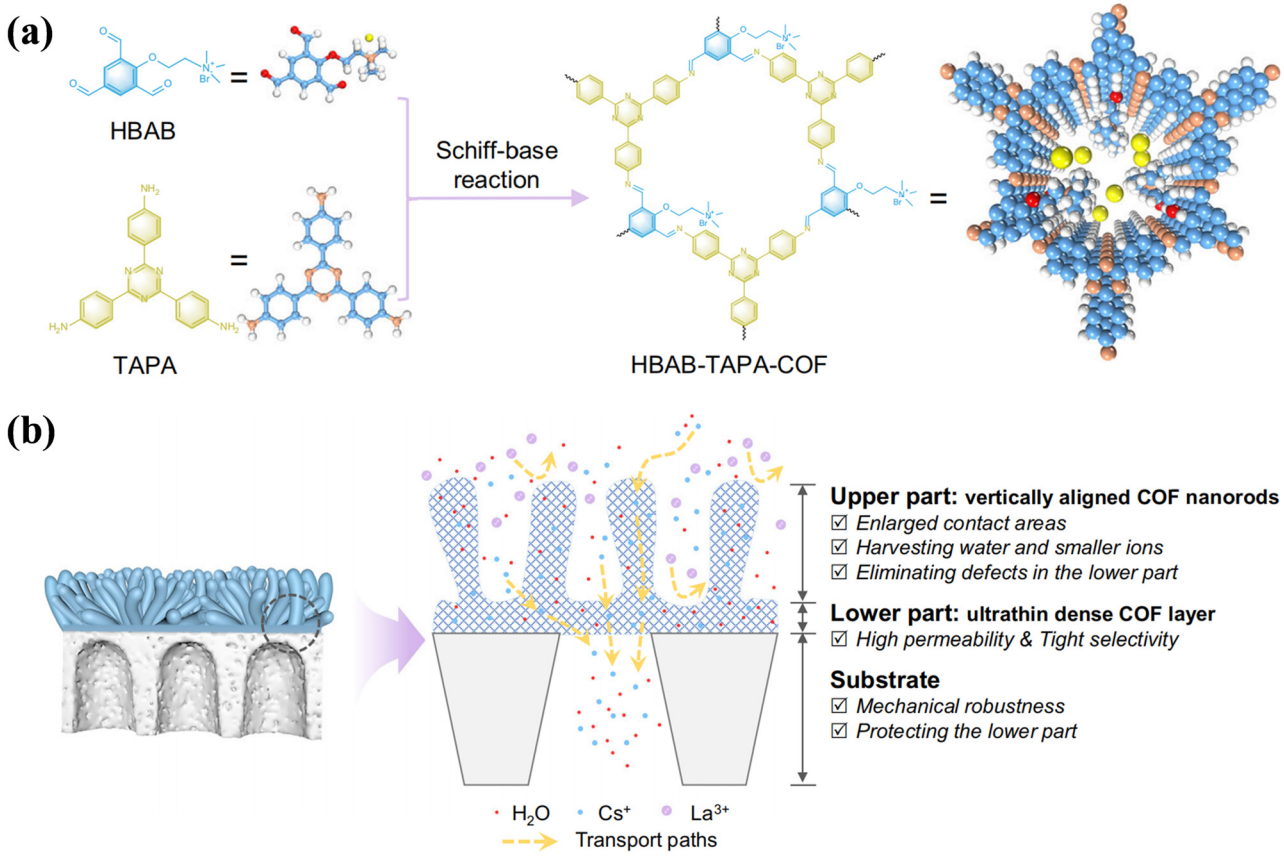

Figure 6: (a) Schematic of the HBAB-TAPA-COF synthesis route and (b) illustration of the asymmetric structure of the COF membrane [43].

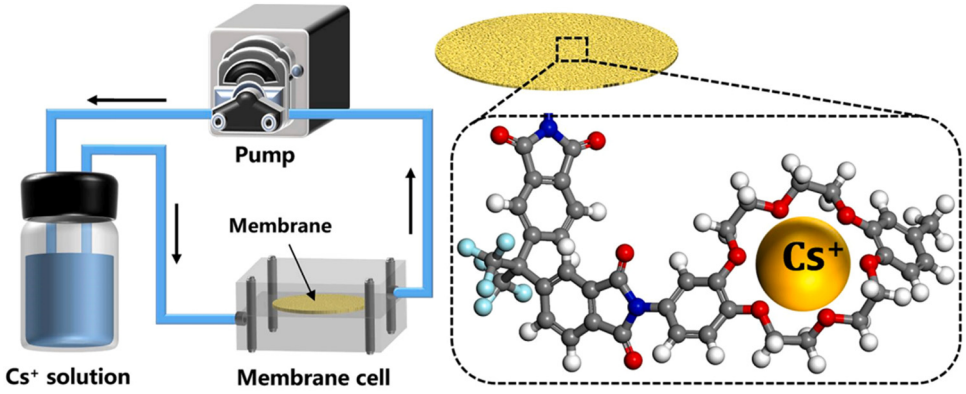

Figure 7: Experimental adsorption setup and proposed adsorption mechanism [45].

selectivity, superior thermal stability, simple process, and operational convenience. Common adsorbents include aluminosilicates, polyoxometalates (POMs), polyvalent metal acid salts, ferrocyanides, ferricyanides, and titanate-based adsorbents.

2.4.1 Aluminosilicates

Aluminosilicates are typically colorless crystals with large specific surface areas and multidimensional pore channel structures. Their key feature lies in the partial substitution of Si^{4+} by Al^{3+} in the silicate framework. To maintain overall charge neutrality, alkali metal ions can be embedded in the lattice to offset excess negative charges. Due to the free mobility of these alkali metal ions within the lattice, aluminosilicates exhibit excellent ion exchange properties. Zeolites are the most representative aluminosilicates, with a general formula of $M_xD_y[Al_{x+2y}Si_{n-(x+2y)}O_{2n}]\cdot mH_2O$ (where M is an alkali metal or monovalent cation and D is an alkaline earth metal or divalent cation). Rajec and Domianová [47] investigated the exchange reactions and adsorption behavior of Cs^+ on natural and modified clinoptilolite, revealing rapid Cs^+ adsorption on clinoptilolite, with K^+ and Na^+ as the primary exchange ions. Munthali *et al.* [48] studied the adsorption selectivity of four zeolites for radioactive Cs^+ and Sr^{2+}, demonstrating that mordenite exhibited the highest Cs^+ selectivity. In simulated soil decontamination experiments using Cs^+-contaminated vermiculite, mordenite achieved a purification efficiency exceeding 90%. Qian *et al.* [49] combined two biomass-derived carbons with potassium titanium silicate to extract Rb^+ and Cs^+ from lepidolite leachate, achieving adsorption capacities of 2.57 $mmol\cdot g^{-1}$ for Rb^+ and 2.12 $mmol\cdot g^{-1}$ for Cs^+. Khandaker *et al.* [50] synthesized a novel zeolite adsorbent *via* hydrothermal modification of municipal sewage sludge slag for Cs^+ removal from simulated wastewater. The optimized material demonstrated a maximum Cs^+ adsorption capacity of 51.02 $mg\cdot g^{-1}$, providing insights into low-cost, high-efficiency adsorbents for radioactive wastewater treatment.

Aluminosilicates are naturally abundant, cost-effective, and exhibit high adsorption capacities for Rb^+ and Cs^+, making them attractive sorbents for separating and enriching these ions from dilute solutions. Nonetheless, effective post-adsorption desorption of Rb^+ and Cs^+ remains challenging, thus limiting their practical applications.

2.4.2 POMs

POMs can be classified into isopolyoxometalates and heteropolyoxometalates. Heteropolyoxometalates are compounds with unique structures and properties, typically formed by heteroatoms (*e.g.*, P, Si, Fe, Co) and polyatoms (*e.g.*, Mo, W, V, Nb, Ta) bridged *via* oxygen coordination, belonging to the family of oxygen-containing polyacids. Their general formula is $M_mXY_{12}O_{40}$, where M represents alkali metal elements, X denotes heteroatoms (*e.g.*, P, As, Si, Co), and Y represents polyatoms (*e.g.*, Mo, W, V, Nb, Ta). These compounds often adopt the Keggin structure and exhibit excellent ion exchange properties. Their affinity for alkali metal ions follows the order: $Cs^+ > Rb^+ > K^+ > Na^+ > Li^+$. Among them, ammonium phosphomolybdate (AMP), with a hollow cage-like structure, demonstrates stronger binding capacity for larger alkali metal ions. Compared to other adsorbents, AMP shows higher selectivity for Rb^+ and Cs^+. Ye *et al.* [51] fabricated a composite spherical adsorbent using AMP, sodium alginate, and calcium chloride. This porous adsorbent achieved rapid adsorption with capacities of 0.58 $mmol\cdot g^{-1}$ for Rb^+ and 0.69 $mmol\cdot g^{-1}$ for Cs^+. Park *et al.* [52] developed an

AMP-PAN composite adsorbent for removing cobalt, strontium, and cesium from radioactive wastewater in nuclear power plants. Results revealed high selectivity for Cs^+, with a maximum adsorption capacity of 0.61 mmol·g^{-1}. Lian *et al.* [53] synthesized a PMA@PCN-224 hybrid by incorporating AMP into a metal–organic framework (MOF) through hydrothermal treatment. The adsorbent reached capacities of 107 mg·g^{-1} for Rb^+ and 128 mg·g^{-1} for Cs^+, and could be rapidly regenerated with NH_4NO_3. This regeneration produced a $CsNO_3$ eluate that yielded high-purity cesium nitrate after a simple purification step. After five adsorption–desorption cycles, the uptake efficiencies for both Rb^+ and Cs^+ remained above 90%. Wang *et al.* [54,55] prepared a Fe_3O_4@ZIF-8@AMP magnetic composite adsorbent, showing 1.86-fold higher adsorption capacity and 2.5-fold faster kinetics compared to powdered AMP. NH_4^+ in AMP undergoes ion exchange with Rb^+ and Cs^+, immobilizing these ions on the material surface. Figure 8(a) and (b) demonstrates increased NH_4^+ concentration and decreased Rb^+/Cs^+ levels during adsorption, confirming the ion exchange mechanism. Additionally, Fe_3O_4 magnetic particles enable efficient solid–liquid separation *via* magnetic fields. Building on this design, the authors synthesized a Fe_3O_4@ZIF-8@AWP core–shell composite. Its adsorption proceeds by two cooperative pathways (Figure 8c): (i) size-selective confinement of Rb^+ and Cs^+ within the cage-like pores of ZIF-8 and (ii) exchange of NH_4^+ in AMP with the target ions. The synergy between physical trapping and chemical exchange endows the composite with high capacity, excellent selectivity, and good recyclability, making it a promising candidate for recovering Rb^+ and Cs^+ from aqueous media.

POMs are attractive sorbents for $^{137}Cs^+$ in high-level radioactive waste because they are easy to synthesize, inexpensive, and highly selective. In practice, however, their microcrystalline powder form generates large pressure drops, channelling, and clogging in fixed-bed columns, hindering scale-up. These drawbacks can be mitigated by immobilizing POMs on porous supports – such as MOFs or hydrogels – or within magnetic matrices like Fe_3O_4@ZIF-8. The resulting composites offer greater mechanical stability, faster mass transfer, and more efficient post-separation handling.

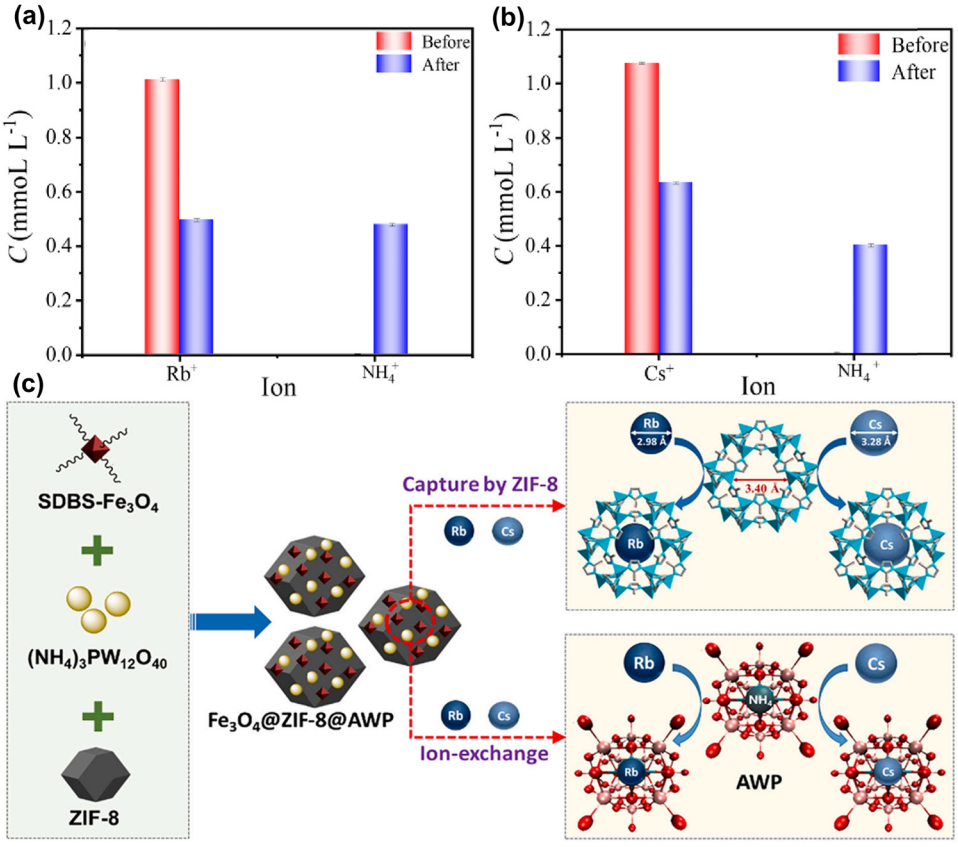

Figure 8: (a) Concentration changes of Rb^+ and NH_4^+ before and after adsorption [54], (b) concentration changes of Cs^+ and NH_4^+ before and after adsorption [54], and (c) mechanism of Rb^+ and Cs^+ adsorption on Fe_3O_4@ZIF-8@AWP (NH^{4+} particle size = 3.5 Å) [55].

2.4.3 Polyvalent metal acid salts

Polyvalent metal acid salts (*e.g.*, titanium phosphate [TiP] and zirconium phosphate [ZrP]) have garnered significant attention in rubidium and cesium separation due to their simple synthesis, excellent chemical stability, strong ion selectivity, and high exchange capacity. These materials typically feature stable frameworks formed by polyvalent metal cations and acidic anions (*e.g.*, PO_4^{3-}) *via* coordination. For instance, TiP and ZrP, as early-stage adsorbents, have been successfully applied to efficiently remove ^{137}Cs from highly acidic radioactive waste. Kapnisti *et al.* [56] systematically evaluated the uptake of cesium in aqueous solutions of pH 5 by TiP in the presence and absence of a background electrolyte. As illustrated in Figure 9a, introducing 0.1 mol·L^{-1} Na^+ reduced the equilibrium capacity from 166.7 to 118.4 mg·g^{-1}, indicating that Na^+ competes for the active exchange sites and thereby diminishes adsorption performance. Maslova *et al.* [57] synthesized TiP materials *via* a heterogeneous reaction of $(NH_4)_2TiO(SO_4)_2{\cdot}H_2O$ with phosphoric acid, demonstrating a Cs^+ adsorption capacity of 1.38 mmol·g^{-1} at 25°C. Despite their superior selectivity, polyvalent metal phosphates remain limited by insufficient adsorption capacities. Notably, Wu *et al.* [58] achieved a breakthrough in trace cesium treatment using zirconium–titanium phosphate composite. Experimental data revealed that this material maintained high adsorption efficiency even at 500 ppb Cs^+ levels, with ^{137}Cs removal rates reaching 98.3% in both deionized water and seawater systems. In a pilot-scale slurry-bed unit, it maintained 92.7% removal after 12 consecutive cycles (Figure 9b).

To address this limitation, researchers have proposed strategies to construct highly stable pyrophosphates by introducing pyrophosphate ($P_2O_7^{4-}$). For example, Wang *et al.* [59] developed a spherical composite adsorbent (PVC-SSbPP, where SSbPP denotes tin–antimony pyrophosphate) using polyvinyl chloride (PVC) as a carrier. At a

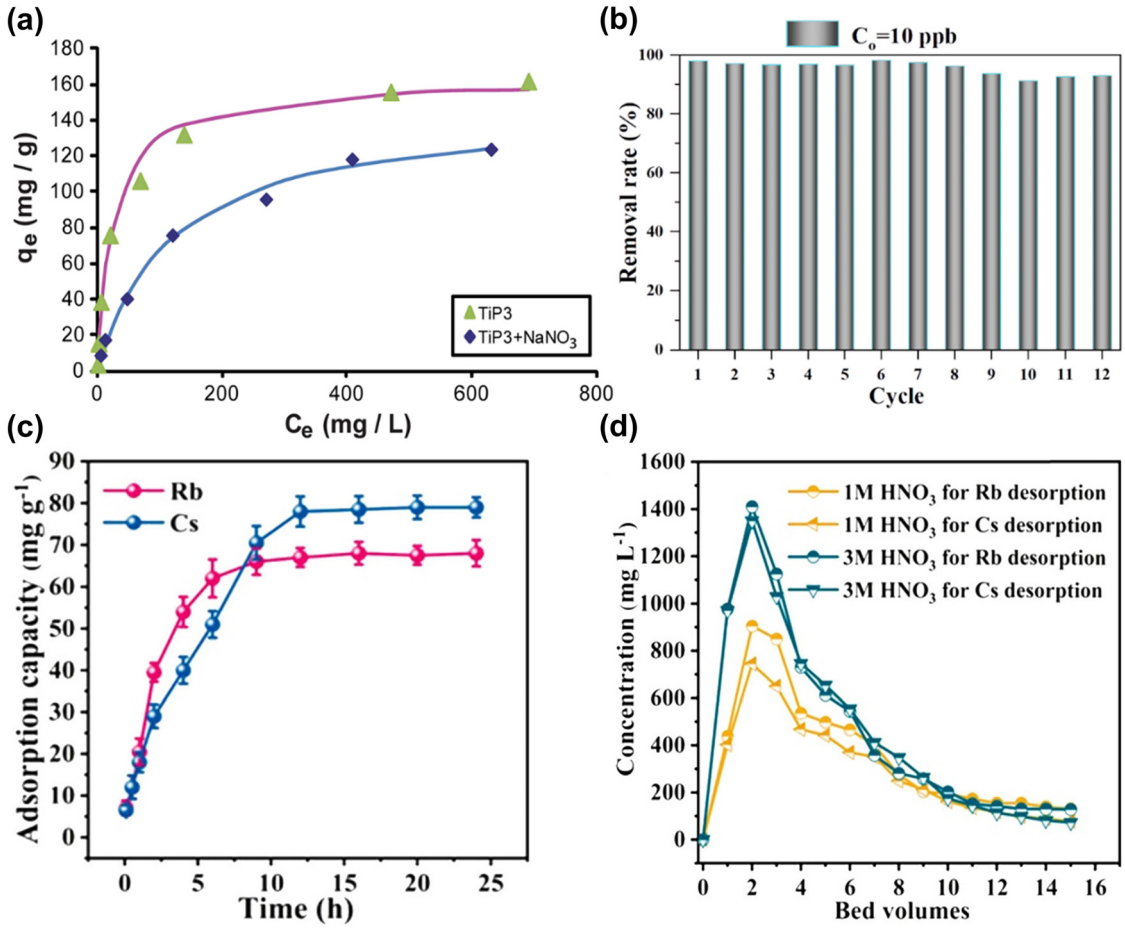

Figure 9: (a) Comparison of adsorption isotherms of cesium ions onto TiP_3 in the absence and presence of 0.1 mol·L^{-1} $NaNO_3$ at pH 5 [56]. (b) Pilot-scale adsorption with 10 ppb feed solution [58]. (c) Effect of adsorption time on PVC-SSbPP [59]. (d) Dynamic elution curves of Rb^+ and Cs^+ from the adsorbent at different desorption solution concentrations [59].

Sn:Sb:P molar ratio of 0.5:0.25:2, the composite reached equilibrium capacities of 68 $mg \cdot g^{-1}$ for Rb^+ and 79 $mg \cdot g^{-1}$ for Cs^+ (Figure 9c). Fixed-bed tests showed that higher HNO_3 concentrations accelerated desorption and that PVC-SSbPP concentrated Rb^+ and Cs^+ from 10 $mg \cdot L^{-1}$ feed solutions by roughly 140-fold (Figure 9d). These results identify PVC-SSbPP as a green, efficient sorbent for recovering trace rubidium and cesium from high-salinity streams.

Polyvalent metal acid salts (*e.g.*, TiP, tin–antimony pyrophosphate) offer significant advantages for the separation of rubidium and cesium owing to their tunable synthesis, outstanding chemical stability, and high selectivity. However, practical applications remain constrained by limited adsorption capacity imposed by their rigid frameworks, performance degradation in highly acidic and saline media, and low separation efficiency caused by the nearly identical physicochemical properties of Rb^+ and Cs^+. Therefore, efficient recovery of rubidium and cesium from dilute solutions remains challenging.

2.4.4 Ferrocyanide and ferrous ferrocyanide-based adsorbents

Transition metal hexacyanoferrates are a class of coordination compounds with remarkable ion exchange properties, represented by the general formula $A_xM[Fe(CN)_6]\cdot 6H_2O$ (A: alkali metal cation; M: transition metal cation, *e.g.*, Fe, Co, Ni, Cu). Owing to their straightforward synthesis, low cost, and high chemical stability, these materials are highly promising sorbents for Cs^+.

Yang *et al.* [60] successfully synthesized hollow flower-like titanium ferrocyanide (hf-TiFC) based on the Kirkendall effect, which demonstrated superior adsorption kinetics, saturation capacity, and selectivity for ^{137}Cs compared to conventional

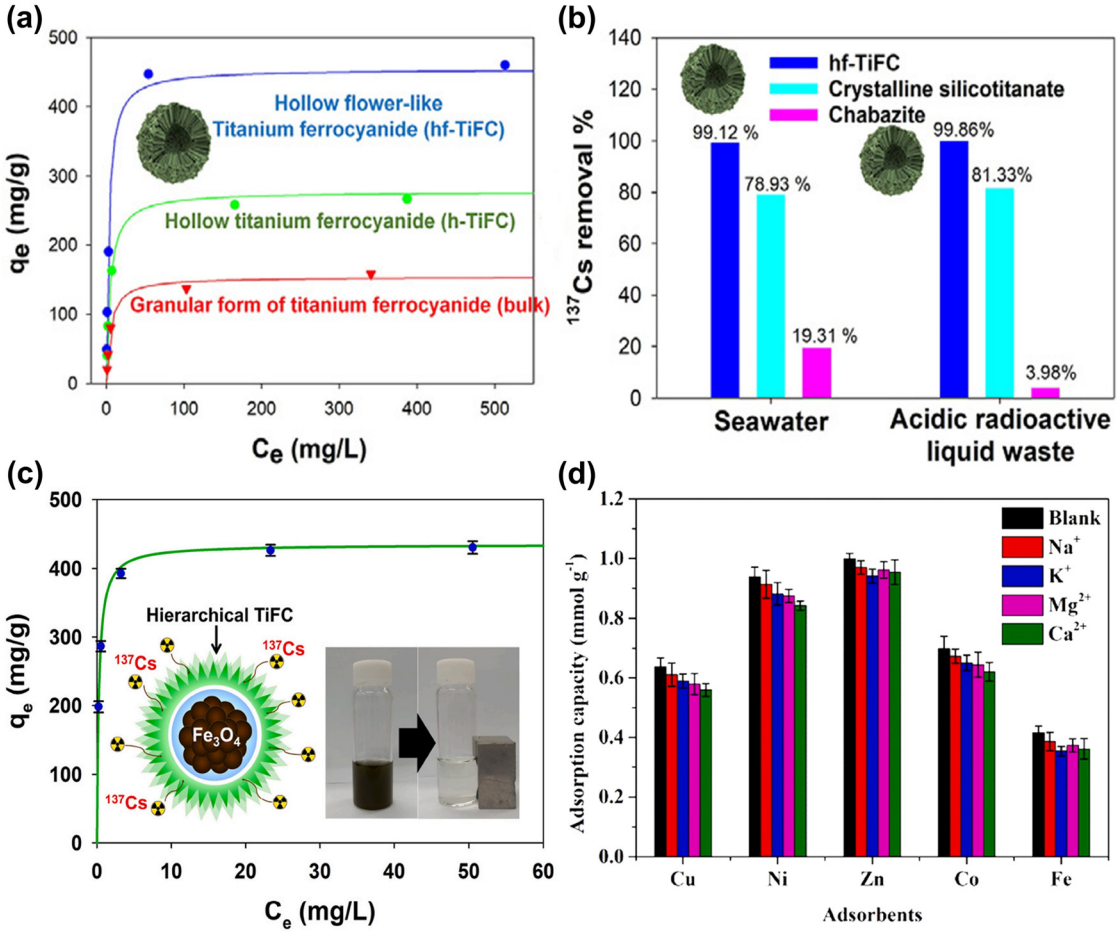

Figure 10: (a) Adsorption performance of hf-TiFC [60]. (b) Adsorption performance of different adsorbents in simulated seawater and acidic radioactive waste solutions [60]. (c) Adsorption performance of mh-TiFC with a hierarchical structure [62]. (d) Effects of competing cations on the Cs^+ adsorption capacity of the adsorbents [63].

TiFC. Its maximum capacity reached 454.5 $mg \cdot g^{-1}$, surpassing hollow TiFC (277.8 $mg \cdot g^{-1}$) and granular TiFC (153.9 $mg \cdot g^{-1}$) (Figure 10a). In simulated seawater and nuclear-waste matrices, hf-TiFC maintained >99.1% removal of ^{137}Cs (Figure 10b). Further advancements were achieved by Li *et al.* [61], who developed a PB analogue with Fe–Co framework (PBAFe). By engineering an enlarged specific surface area (452.8 $m^2 \cdot g^{-1}$) and optimized pore size distribution, this material attained an enhanced Cs^+ adsorption capacity of 82.90 $mg \cdot g^{-1}$, achieving 98.57% removal efficiency for cesium ions in radioactive wastewater treatment.

To address the technical limitations of single-component ferrocyanides in mechanical stability, ion exchange capacity, and large-scale column operation efficiency, researchers are actively developing composite ferrocyanide systems. Current composite materials include magnetic matrices, mesoporous materials, carbon nanotubes, and organic substrates. For example, Yang *et al.* [62] prepared a core–shell magnetic adsorbent (mh-TiFC; Figure 10c). mh-TiFC showed the highest reported Cs^+ capacity among magnetic systems (434.8 $mg \cdot g^{-1}$) and could be separated magnetically, removing 99.85% of ^{137}Cs at 22 ppt. Dong *et al.* [63] synthesized a series of KMeFC/Al-MCM-41 (Me = Cu, Ni, Zn, Co, Fe) composite adsorbents using kaolinite-derived Al-MCM-41 mesoporous materials as carriers (Figure 10d). Among these, the KCuFC/Al-MCM-41 composite exhibited a surface area of 685.8 $m^2 \cdot g^{-1}$ and a Cs^+ capacity of 1.16 $mmol \cdot g^{-1}$, maintained high selectivity in multication solutions and reached equilibrium within 10 min owing to K^+/Cs^+ exchange in the carrier framework. Naeimi and Faghihian [64] designed MOF/KNiFC and MOF/Fe_3O_4/KNiFC hybrid materials, combining the structural tunability of MOFs with the magnetic responsiveness of Fe_3O_4. These hybrids retained adsorption capacities of 109–153 $mg \cdot g^{-1}$ while enabling rapid solid–liquid separation under external magnetic fields. Yang *et al.* [65] fabricated a three-dimensional porous composite aerogel photothermal adsorbent (designated as CS/WLSH/C/PBAs). This innovative material leverages the synergistic photothermal conversion properties of PBAs and biochar, where localized heating effects significantly enhance solution enrichment of Cs^+ and Sr^{2+} while strengthening their interfacial interactions with the adsorbent. Under simulated solar irradiation, the composite achieves a maximum Cs^+ adsorption capacity of 156 $mg \cdot g^{-1}$, with the adsorption equilibrium time remarkably reduced from 5 h (dark conditions) to 2 h. This breakthrough establishes a novel strategy for solar-enhanced adsorption efficiency of Cs^+ and Sr^{2+} through photothermal activation mechanisms. Ferrocyanides remain the most widely used

Table 4: Summary of recent studies on the separation of rubidium and cesium using ferrocyanide adsorbents

Adsorbents	Source	Condition	Adsorption capacity ($mg \cdot g^{-1}$)	Ref.
KMgFC	Lithium extraction tailing	c_{Cs^+} = 0.22 $g \cdot L^{-1}$ c_{Rb^+} = 4.68 $g \cdot L^{-1}$ T = 80°C, t = 40 min pH = 8.1	$q_{e(Cs^+)}$ = 8.11 $q_{e(Rb^+)}$ = 158.91	[66]
PAN-KCuFC-PEG	Qarhan salt lake brine	c_{Cs^+} = 65 $mg \cdot L^{-1}$ c_{K^+} = 26,000 $mg \cdot L^{-1}$ pH = 6.4 c_{Cs^+} = 65 $mg \cdot L^{-1}$	$q_{e(Cs^+)}$ = 30.62	[67]
MKNiCuFC@ZIF-8	Simulated brine	c_{Rb^+} = 10 $mg \cdot L^{-1}$ pH = 8, T = 45°C	$q_{e(Rb^+)}$ = 246.3	[68]
KCoFC-HPR	Simulated brine	c_{Rb^+} = 5 $mg \cdot L^{-1}$ pH = 8, T = 25°C, t = 24 h	$q_{e(Rb^+)}$ = 211.2	[69]
MKCoFC	Simulated brine	c_{Rb^+} = 10 $mg \cdot L^{-1}$ pH = 8, T = 45°C, t = 24 h	$q_{e(Rb^+)}$ = 208.8	[70]
GPSC-KCuFC	Qinghai saline lake	c_{Rb^+} = 10 $mg \cdot L^{-1}$ pH = 6.5, t = 6 h	$q_{e(Rb^+)}$ = 30.7	[71]
KCoFC@ZIF	Seawater	c_{Rb^+} = 5 $mg \cdot L^{-1}$ pH = 7.0	$q_{max(Rb^+)}$ = 1279.35	[72]
CuFC-MAM	Simulated radioactive solutions	c_{Cs^+} = 21.25 ppt	Removal rate > 99%	[73]
PAN/PB	Simulated radioactive solutions	c_{Cs^+} = 10 ppm pH = 8	$q_{e(Cs^+)}$ = 152.67	[74]
PBA/CS/CNTs	Simulated radioactive solutions	c_{Cs^+} = 200 $mg \cdot L^{-1}$ pH = 6, T = 20°C, t = 6 h	$q_{e(Cs^+)}$ = 219.8	[75]

sorbents for rubidium–cesium separations. Table 4 summarizes recent studies employing these materials.

2.4.5 Titanium silicate-based adsorbents

Titanium silicates are a novel class of inorganic ion exchangers, with basic structural units formed by TiO_6 octahedra or TiO_5 pentagonal bipyramids connected to SiO_4 tetrahedra *via* oxygen bridges. The negative charges on Ti–O groups are balanced by exchangeable cations. Depending on the spatial arrangement of these units, titanium silicates can adopt three-dimensional frameworks, layered structures, or dense configurations. Among these, layered titanium silicates exhibit the highest ion exchange and adsorption capacities. Clearfield *et al.* [76] systematically investigated the ion-exchange properties of framework-type titanium silicates ($M_2Ti_2O_3SiO_4{\cdot}nH_2O$, M = H, Na), revealing an affinity order for heavy alkali metal ions of $Cs^+ > Rb^+ > K^+$. This unique selectivity arises from the optimal match between Cs^+ ionic diameter and the interlayer cavity size of titanium silicates, making them highly valuable for nuclear waste treatment, environmental remediation, and biofluid purification. Liu *et al.* [77] developed two layered titanium silicates, ETS-1 and ETS-2, and evaluated their adsorption performance for Cs^+ and Sr^{2+}. While ETS-1 showed superior Cs^+ adsorption, it lacked selectivity for Cs^+. Perovskiy *et al.* [78] innovatively synthesized a sodium titanosilicate with the sitinakite structure using quartz-leucoxene concentrate processing waste (Figure 11), achieving both high-value utilization of industrial solid waste and a remarkable Cs^+ adsorption capacity of 170 $mg{\cdot}g^{-1}$, highlighting its eco-friendly characteristics. Eom *et al.* [79] integrated a dicationic titanium silicate (DTS) with capacitive deionization technology to develop an electrochemical adsorption system for selective removal of radioactive Cs^+ and Sr^{2+}. The DTS-modified electrode achieved adsorption equilibrium within 30 min, with a Cs^+ adsorption capacity of 186 $mg{\cdot}g^{-1}$.

2.4.6 Layered alkali titanate adsorbents

Layered titanates are a class of cationic-layered compounds with unique open-framework layered crystal structures. Their general formula is $A_2Ti_nO_{2n+1}$ ($n \geq 1$, where A is a monovalent alkali metal). Structurally, they consist of negatively charged layered frameworks formed by TiO_6 octahedral layers, with interlayer cations balancing the charge and holding the layers together *via* Coulombic forces [80]. These materials feature tunable interlayer spaces capable of accommodating ions of varying sizes, along with excellent acid/alkali resistance and radiation stability, making them ideal for ion exchange applications [81]. Recent advances in layered titanate-based adsorbents

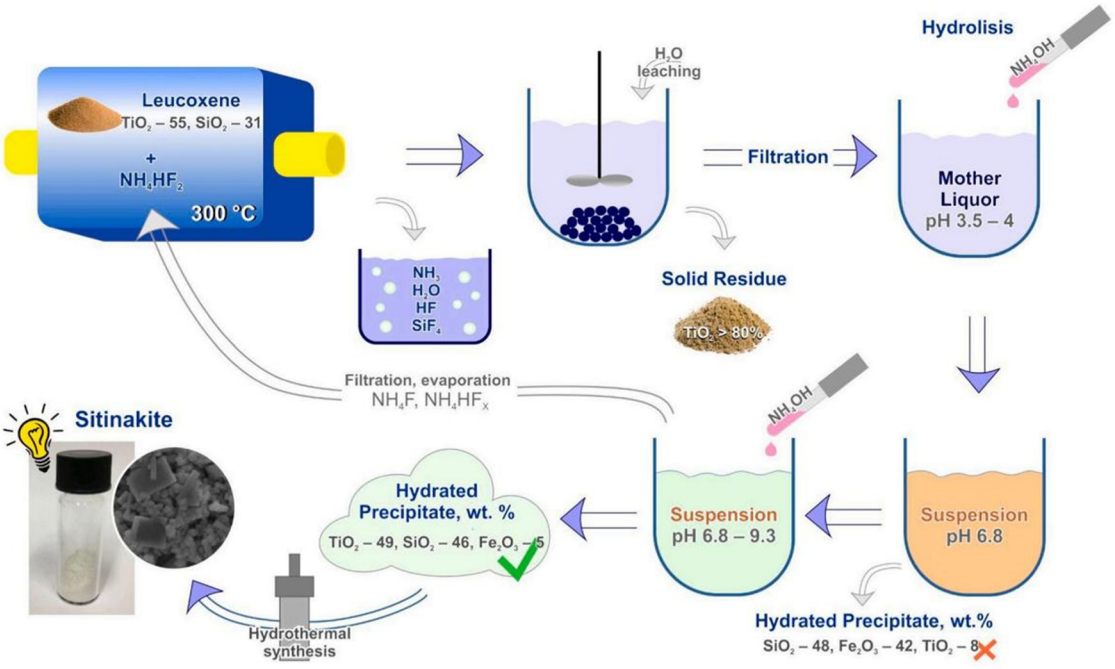

Figure 11: Synthesis flowchart of sodium titanosilicate from quartz-leucoxene concentrate [78].

have been notable. Liu *et al.* [82] successfully loaded $Na_2Ti_3O_7$ onto a three-dimensional carbon aerogel to prepare a CA/$Na_2Ti_3O_7$ composite adsorbent and investigated its adsorption performance for Rb^+ and Cs^+. Compared to pure $Na_2Ti_3O_7$, the composite exhibited both higher adsorption capacity and significantly reduced adsorption equilibrium time. Li *et al.* [83] used a hydrothermal method to deposit sodium titanate and potassium titanate onto biomass-derived carbon aerogels. The resulting materials – NBCA, NCBCA, KBCA, and KCBCA – exhibited markedly higher Rb^+ and Cs^+ uptakes than the unmodified BCA and CBCA (Figure 12a). The improvement is attributed to efficient ion exchange between surface Na^+/K^+ sites and Rb^+/Cs^+ in solution.

To further enhance the performance, Amesh *et al.* [84] introduced Fe^{3+} doping into sodium titanate, expanding its cavity structure to improve Cs^+ accommodation. Optimizing the Ti/Fe ratio significantly enhanced selective Cs^+ adsorption. Although adsorbed Cs^+ could be regenerated *via* nitric acid elution, the long-term cycling stability requires further validation.

Addressing the challenges in regeneration and recycling of titanate adsorbents, Geng *et al.* [85,86] conducted systematic studies. They synthesized precursor $Cs_2Ti_6O_{13}$ (CTO) *via* sol–gel and solid-phase sintering methods, followed by acid modification to produce protonated titanate (H-CTO). H-CTO displayed a maximum Cs^+ capacity of 329 $mg \cdot g^{-1}$ and still retained 85% of its initial capacity (281 $mg \cdot g^{-1}$) after five adsorption–desorption cycles (Figure 12b). The TiO_6 octahedra carry a net negative charge; upon acid modification, exchangeable H^+ ions bind to terminal oxygen to form –OH groups dispersed between the layers. During acid treatment, surface –OH groups are created and O–Cs bonds are broken, whereas Cs^+ uptake proceeds *via* cleavage of these –OH groups and formation of new O–Cs bonds (Figure 12c). Further

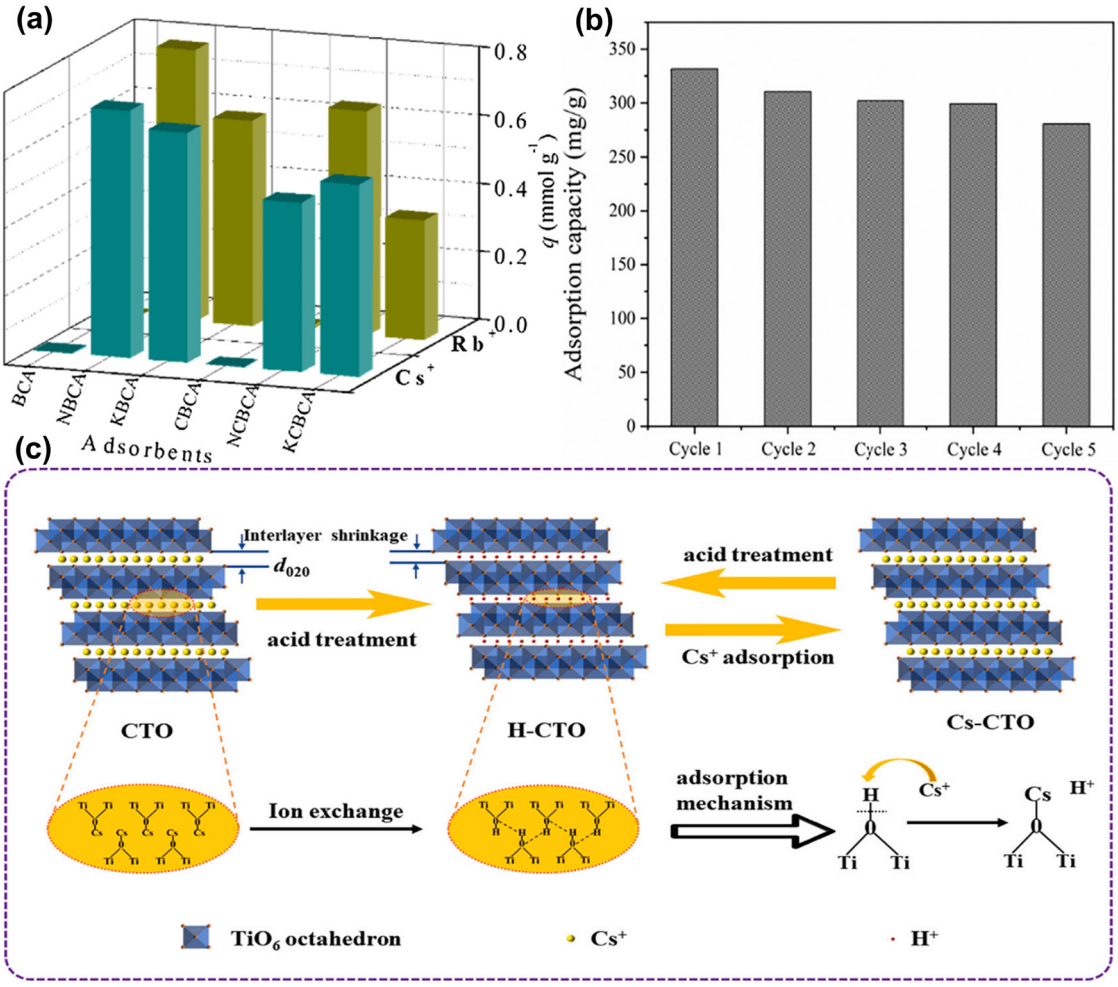

Figure 12: (a) Adsorption capacities of BCA and NBCA before and after modification with sodium titanate or potassium titanate [83]. (b) Cs^+ adsorption performance of H-CTO over five adsorption–elution cycles [85]. (c) Proposed mechanism for Cs^+ adsorption by the H-CTO adsorbent [85].

optimizing the synthesis, the team prepared HTO/PMMA *via* sol–gel and/template-free methods. Compared to sol–gel-derived sieves, HTO/PMMA showed an increased adsorption capacity (from 224.32 to 299.15 $mg \cdot g^{-1}$) and a specific surface area of 67.282 $m^2 \cdot g^{-1}$, providing abundant ion-exchange sites for Cs^+. Yang *et al.* [87] developed $H_2Ti_6O_{13}$ that modulates the surface morphology and hydrophilicity of the precursor by F127 and cetylamine, and the specific surface area of HTO-3 can reach 42.929 $m^2 \cdot g^{-1}$ compared to that of the unmodified ionic sieve HTO-2 (33.548 $m^2 \cdot g^{-1}$). The adsorption mechanism of Cs^+ on the HTO-3 ion sieve involves two key steps, as illustrated in Figure 13. Acid washing first cleaves the O–Cs bonds in the precursor $Cs_2Ti_6O_{13}$ (CTO-3), producing surface –OH groups and converting CTO-3 to HTO-3. When HTO-3 contacts a Cs^+ solution, the cations bind to these –OH sites, reforming O–Cs bonds while releasing H^+ into the liquid phase. This ion-exchange process completes the adsorption of Cs^+.

In summary, cesium titanate ion-sieves integrate the excellent stability, corrosion resistance, and radiation tolerance inherent to titanate-based adsorbents with the exceptional ion selectivity and adsorption capacity characteristic of ion-sieve materials. These combined advantages thus establish them as compelling candidates for efficient separation of rubidium and cesium.

2.5 Other novel adsorbent systems

Beyond traditional inorganic ion-exchange materials, novel adsorbent systems such as todorokite, functionalized cellulose, and magnetic nanomaterials have demonstrated unique advantages in rubidium and cesium separation. However, research on these materials remains in the laboratory exploration stage, and their practical application potential requires further validation. For mineral-based adsorbents, Chitrakar *et al.* [88] systematically investigated modification strategies for todorokite and their Cs^+ adsorption performance. Three modified materials were prepared *via* acid treatment: magnesium-protonated (Mg-H), calcium-protonated (Ca-H), and iron-doped (Fe-Mg-H) types. Experiments revealed that Mg-H and Ca-H exhibited significantly higher Cs^+ adsorption capacities and distribution coefficients than Fe-Mg-H. Notably, Cs^+ desorption efficiency reached 98% in 1 $mol \cdot L^{-1}$ NH_4Cl solution, indicating excellent regeneration potential, though cycling stability has yet to be systematically studied. In functionalized nanomaterials, Liu *et al.* [89] developed a magnetic nano-adsorbent (Fe_3O_4@R–COOH) modified with 18-crown-6 ether. The crown ether functional groups were grafted onto carboxylated Fe_3O_4 nanoparticles *via* amidation, achieving exceptional Cs^+ adsorption performance (q_{max} = 24.25 $mg \cdot g^{-1}$) and superparamagnetism. Density functional theory calculations elucidated the coordination mechanism: Cs^+ is immobilized primarily through chelation with six oxygen atoms on the crown ether ring, with binding energies indicating a spontaneous exothermic process. Theoretical analyses further confirmed that adsorption behavior is synergistically governed by crown ether cavity size and coordination symmetry. Chen *et al.* [90] synthesized a 2D/2D stacked Na^+-MXene/layered double hydroxide (LDH) composite through *in situ* growth of LDH on MXene surfaces. This architecture achieved a remarkable Cs^+ adsorption capacity of 961.538 $mg \cdot g^{-1}$. When tested in brine from Dongtai Jinaier Salt Lake (Qinghai, China), the composite demonstrated a distribution coefficient of 31.92 × 10^4 $mL \cdot g^{-1}$, highlighting its high affinity and selectivity for Cs^+. Xu *et al.* [91] engineered three self-condensed hypercrosslinked polymers (HCP-HBAs) *via* hydroxyl substitution at ortho-, meta-, and para-positions of commercial benzyl alcohol. Among these, HCP-o-HBA exhibited the highest Cs^+ adsorption capacity (302.1 $mg \cdot g^{-1}$) with an exceptional Cs^+/K^+ separation factor of 44.7. This material shows promising potential for high-efficiency, selective cesium extraction from brines and wastewater systems.

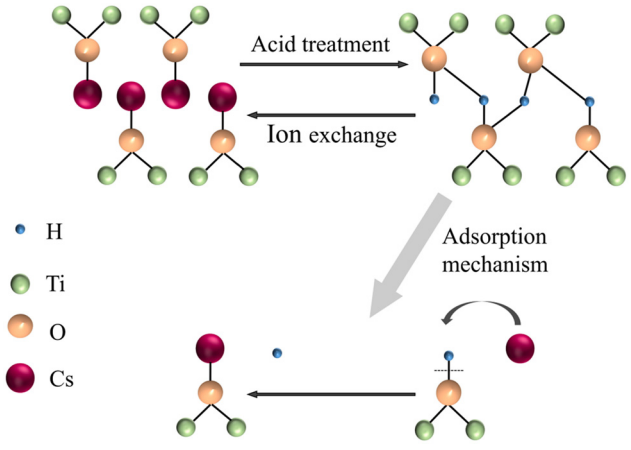

Figure 13: Mechanism of cesium ion adsorption [87].

Adsorption offers a simpler and more environmentally benign route than precipitation or solvent extraction, and is therefore regarded as one of the most promising strategies for recovering rubidium and cesium from salt-lake brines. Table 5 summarizes the main strengths and weaknesses of the principal adsorbent families. In practice, however, complex feed chemistries and the intrinsic physicochemical similarity of Rb^+ and Cs^+ impose several hurdles. Real brines often display slow ion-exchange kinetics,

poor desorption and regeneration, and reduced selectivity due to competition from co-existing ions with large hydration shells. These challenges have so far confined most adsorption studies to the laboratory scale.

3 Conclusions and outlook

3.1 Conclusions

Current rubidium and cesium extraction technologies primarily encompass precipitation, solvent extraction, membrane separation, and adsorption methods. While precipitation is a mature process, it suffers from high-energy consumption, significant reagent usage, and limited applicability to high-concentration rubidium and cesium solutions. Solvent extraction, as the mainstream industrial method, offers advantages such as high throughput and separation efficiency but faces challenges including costly extractants, severe equipment corrosion, and organic phase loss. Membrane materials are prone to fouling, aging, or damage, compromising separation efficiency and lifespan. In contrast, adsorption methods exhibit unique advantages in low-concentration resource recovery due to their low energy consumption, high selectivity, and environmental friendliness. However, existing adsorbents are hindered by technical bottlenecks such as poor mechanical strength, limited cycling stability, and inefficient elution, which restrict their industrial-scale application.

3.2 Outlook

With the rapid development of strategic emerging industries (*e.g.*, renewable energy, electronics), global demand for rubidium and cesium is projected to grow at an annual rate of 8–10%. To address these challenges, future innovations in rubidium and cesium separation technologies should focus on the following directions:

1) Innovative design of green functional materials. Developing novel adsorbents is critical for enhancing separation efficiency, particularly porous framework materials (*e.g.*, MOFs and COFs) and bioinspired mineral materials. Tailoring pore size and structure can improve rubidium and cesium selectivity and adsorption capacity. Magnetic-mesoporous hybrid materials and biomass-based composites also offer promising avenues for green synthesis and high-efficiency adsorption.
2) Synergistic integration of technologies and intelligent control. Establishing integrated "adsorption-membrane separation-electrochemical" processes through optimized parameters and workflow design can further enhance rubidium and cesium recovery rates. Incorporating machine learning algorithms and big data analytics to develop intelligent process control systems will enable real-time optimization and precise regulation, improving stability and reliability.
3) Efficient utilization of low-grade resources. As rubidium and cesium resources become increasingly scarce, efficient extraction from low-grade sources (*e.g.*, salt lake brines, seawater) is imperative. Developing ultra-selective ion-exchange membranes and capacitive deionization materials, along with nanochannel engineering and surface modification strategies, will maximize recovery from low-concentration systems.

In summary, future advancements in rubidium and cesium separation will prioritize green, intelligent, and resource-efficient approaches. Through synergistic innovation in materials, processes, and equipment, breakthroughs in high-stability adsorbents, intelligent separation systems, and ultra-low-concentration recovery technologies will

Table 5: Advantages and disadvantages of different adsorbents

Type of adsorbent	Advantages	Disadvantages
Aluminosilicates	Low-cost, easy to prepare, and resistant to acid, alkali, and high temperature, suitable for complex systems	Slow ion exchange and difficult desorption hinder efficient regeneration
POMs	Wide pH range, high selectivity for Cs^+ in acidic environments	Microcrystalline form hinders post-adsorption separation
Polyvalent metal acid salts	Exhibits high selectivity for rubidium and cesium ions	Low capacity; unstable in acidic and saline conditions
Prussian blue and its analogs	Low-cost, highly selective, and stable in acidic or neutral environments, suitable for complex systems	Microcrystalline structure with low strength and poor recyclability; often used in composites
Titanium-based adsorbents	Corrosion resistance, radiation resistance, excellent stability, large adsorption capacity	Long adsorption time and higher cost than other adsorbents

establish a sustainable, eco-friendly resource utilization framework, securing critical material supplies for strategic industries.

Acknowledgments: This work was supported by the Qinghai Provincial Key Research and Development (R&D) and Transformation Program (No. 2025-QY-240), the Tianjin University-Qinghai Minzu University Joint Innovation Fund (No. 24TQ003), and the Natural Science Foundation of Qinghai Minzu University (No. 2024XJMA02).

Funding information: This work was supported by the Qinghai Provincial Key Research and Development (R&D) and Transformation Program (No. 2025-QY-240), the Tianjin University-Qinghai Minzu University Joint Innovation Fund (No. 24TQ003), and the Natural Science Foundation of Qinghai Minzu University (No. 2024XJMA02).

Author contributions: All authors have accepted responsibility for the entire content of this manuscript and approved its submission.

Conflict of interest: The authors state no conflict of interest.

Data availability statement: Data sharing is not applicable to this article as no datasets were generated or analysed during the current study.

References

[1] Shi, T. T., Q. Wei, X. M. Qin, Z. F. Liu, K. K. Chen, S. Y. Cao, et al. Dual-frequency optical-microwave atomic clocks based on cesium atoms. *Photonics Research*, Vol. 12, No. 9, 2022, pp. 1972–1980.

[2] Kaczorowska, M. A. Novel and sustainable materials for the separation of lithium, rubidium, and cesium ions from aqueous solutions in adsorption processes – a review. *Materials*, Vol. 17, No. 24, 2024, id. 6158.

[3] Liu, Y. P., Y. Q. Mu, X. H. Yang, Z. Y. Yao, S. F. Peng, J. C. Shi, et al. Properties and factors of Cs_xWO_3 slurry for building glass with high visible light transmission and outstanding near-infrared insulation. *Materials*, Vol. 17, No. 21, 2024, id. 5196.

[4] Joy, J., R. R. Madhavan, S. Sen, D. Sujish, R. Kumaresan, and K. Joseph. Studies on synthesis and properties of zinc doped cesium iron phosphate glasses. *Journal of Non-Crystalline Solids*, Vol. 646, 2024, id. 123233.

[5] Wang, Z., H. J. Luo, L. H. Wang, T. Li, S. R. Li, and Y. Q. Liu. Promotion of low-temperature catalytic activity of Ru-based catalysts for ammonia decomposition via lanthanum and cesium codoping. *ACS Sustainable Chemistry & Engineering*, Vol. 12, No. 14, 2024, pp. 5620–5631.

[6] Khan, A. A., M. Noman, and S. T. Jan. Investigating the compatibility of kesterite and zinc charge transport layers with inorganic germanium perovskite solar cells. *Optical and Quantum Electronics*, Vol. 57, No. 1, 2025, id. 114.

[7] Alsaab, A. H. and S. Zeghib. Study of prepared lead-free polymer nanocomposites for X- and gamma-ray shielding in healthcare applications. *Polymers*, Vol. 15, No. 9, 2023, id. 2142.

[8] Kumar, D. K., N. Ramakrishnan, and V. Swamy. Cesium based inorganic halide perovskite for sensing applications: a review. *Sensors and Actuators A: Physical*, Vol. 381, 2025, id. 115749.

[9] Zhang, Z. Y., F. F. Chen, S. X. Dai, C. G. Lin, T. F. Xu, Q. H. Nie, et al. Synthesis of rubidium lead iodide perovskite nanocrystals in chalcogenide glasses and high nonlinear optical performance of the nanocomposites. *Journal of Alloys and Compounds*, Vol. 1011, 2025, id. 178499.

[10] Xing, P., C. Y. Wang, Y. Q. Chen, and B. Z. Ma. Rubidium extraction from mineral and brine resources: a review. *Hydrometallurgy*, Vol. 203, 2021, id. 105644.

[11] Zhao, L., M. M. Wang, Y. G. Xia, and J. Gao. Research progress on the extraction and separation technology of rubidium and cesium ions. *Journal of Salt Lake Research*, Vol. 32, 2024, pp. 1–9.

[12] Gao, L., G. H. Ma, Y. X. Zheng, Y. Tang, G. S. Xie, J. W. Yu, et al. Research trends on separation and extraction of rare alkali metal from salt lake brine: rubidium and cesium. *Solvent Extraction and Ion Exchange*, Vol. 38, No. 7, 2020, pp. 753–776.

[13] Fang, D. Z., Y. P. Wang, H. N. Liu, H. F. Zhang, X. S. Ye, Q. Li, et al. Efficient extraction of Rb^+ and Cs^+ by a precipitation flotation process with ammonium phosphowolframate as precipitant. *Colloids and Surfaces A: Physicochemical and Engineering*, Vol. 608, 2021, id. 125581.

[14] Li, K., Z. C. Yin, J. Dong, L. L. Xu, Y. S. Liu, R. X. Ma, et al. Separation of Cs^+ from Rb^+ and Cs^+ co-existing solution by $Cs_3Bi_2I_9$ precipitation to produce CsI. *Chemical Engineering Research and Design*, Vol. 197, 2023, pp. 372–379.

[15] Soliman, M. A., G. M. Rashad, and M. R. Mahmoud. Fast and efficient cesium removal from simulated radioactive liquid waste by an isotope dilution-precipitate flotation process. *Chemical Engineering Journal*, Vol. 275, 2015, pp. 342–350.

[16] Lu, J. M., D. Dreisinger, R. McElroy, C. Oloman, B. Downing, and D. Trueman. Cesium extraction from the Taron deposit. *Hydrometallurgy*, Vol. 210, 2022, id. 105823.

[17] Sopapan, P., U. Lamdab, T. Akharawutchayanon, S. Issarapanacheewin, K. Yubonmhat, W. Silpradit, et al. Effective removal of non-radioactive and radioactive cesium from wastewater generated by washing treatment of contaminated steel ash. *Nuclear Engineering and Technology*, Vol. 55, No. 2, 2023, pp. 516–522.

[18] Jiao, C. S., G. H. Wang, J. L. Wang, Y. Gao, H. G. Hou, M. Zhang, et al. Effects of coprecipitation conditions on Cs^+ removal, coprecipitate compositions and coprecipitate particle-size distribution in nickel potassium ferrocyanide systems. *Journal of Radioanalytical and Nuclear Chemistry*, Vol. 330, No. 1, 2021, pp. 293–303.

[19] Li, C. X., K. Li, S. N. Li, and R. X. Ma. Efficient enrichment of rubidium and cesium from high salt solution by copper hexacyanoferrate co-precipitation. *ChemistrySelect*, Vol. 10, No. 8, 2025, id. e202406007.

[20] Kivan, O., M. Yusuf, D. Harbottle, and T. N. Hunter. Removal of cesium and strontium ions with enhanced solid–liquid separation by combined ion exchange and $BaSO_4$ co-precipitation. *Journal of Water Process Engineering*, Vol. 59, 2024, id. 104934.

[21] Kivan, O., M. Yusuf, R. Filson-Halliwell, J. N. Enemmo, D. Harbottle, and T. N. Hunter. Intensified co-precipitation and ion exchange using an agitated tubular reactor (ATR) for enhanced removal of

Cs^+ and Sr^{2+} ions. *Chemical Engineering and Processing*, Vol. 207, 2025, id. 110077.

[22] Jandová, J., P. Dvořák, J. Formánek, and H. N. Vu. Recovery of rubidium and potassium alums from lithium-bearing minerals. *Hydrometallurgy*, Vol. 119, 2012, pp. 73–76.

[23] Lei, Z. W., X. W. Li, P. W. Huang, H. M. Hu, Z. Li, and Q. W. Zhang. Mechanochemical activation of antigorite to provide active magnesium for precipitating cesium from the existences of potassium and sodium. *Applied Clay Science*, Vol. 168, 2019, pp. 223–229.

[24] Stoll, I., J. Eberhard, R. Brodbeck, W. Eisfeld, and J. Mattay. A new fluorescent calix crown ether: synthesis and complex formation with alkali metal ions. *Chemistry: A European Journal*, Vol. 14, No. 4, 2008, pp. 1155–1163.

[25] Wang, L., Y. H. Xiong, X. W. Zhou, L. Xu, Y. P. Tian, and Z. Zhao. Complexation mechanism of crown ethers with rubidium and cesium ions using density functional theory. *Computational & Theoretical Chemistry*, Vol. 1225, 2023, id. 114139.

[26] He, J. T., J. Y. Hua, X. H. Ma, R. Wickramasinghe, and J. X. Li. A mixed solvent system of amino crown ether and ionic liquids for a high-efficient extraction of cesium. *Journal of Molecular Liquids*, Vol. 412, 2024, id. 125868.

[27] Shi, Z., X. M. Du, S. Q. Wang, Y. F. Guo, and T. L. Deng. Application status of rubidium, cesium and research situation of its separation from brine with solvent extraction. *IOP Conference Series: Materials Science and Engineering*, Vol. 274, No. 1, 2017, id. 012081.

[28] Chen, W. S., C. H. Lee, Y. F. Chung, K. W. Tien, Y. J. Chen, and Y. A. Chen. Recovery of rubidium and cesium resources from brine of desalination through t-BAMBP extraction. *Metals*, Vol. 10, No. 5, 2020, id. 607.

[29] Xie, J. J., K. Li, Z. N. Shi, C. L. Min, S. N. Li, Z. C. Yin, et al. Separation of cesium and rubidium from solution with high concentrations of potassium and sodium. *Separations*, Vol. 10, No. 1, 2023, id. 42.

[30] Lv, Y. W., B. Z. Ma, Y. B. Liu, C. Y. Wang, W. J. Zhang, and Y. Q. Chen. Selective extraction of cesium from high concentration rubidium chloride leach liquor of lepidolite. *Desalination*, Vol. 530, 2022, id. 115673.

[31] Lv, Y. W., Y. B. Liu, B. Z. Ma, C. Y. Wang, and Y. Q. Chen. Preferential extraction of rubidium from high concentration impurity solution by solvent extraction and preparation of high-purity rubidium salts. *Desalination*, Vol. 545, 2023, id. 116162.

[32] Chen, X. L. and W. P. Hu. Direct and efficient in situ rubidium extraction from potassium chloride salts. *Nature Sustainability*, Vol. 7, 2024, pp. 1672–1680.

[33] Sachleben, R. A., A. Urvoas, J. C. Bryan, T. J. Haverlock, B. P. Hay, and B. A. Moyer. Dideoxygenated calix[4] arene crown-6 ethers enhanced selectivity for caesium over potassium and rubidium. *Chemical Communications*, Vol. 17, 1999, pp. 1751–1752.

[34] Pang, D. K., Z. H. Zhang, Y. Q. Zhou, Z. H. Fu, Q. Li, Y. M. Zhang, et al. The process and mechanism for cesium and rubidium extraction with saponified 4-tert-butyl-2-(α-methylbenzyl) phenol. *Chinese Journal of Chemical Engineering*, Vol. 46, 2022, pp. 31–39.

[35] Zhang, X. F., Z. F. Qin, T. Aldahri, S. Rohani, S. Ren, and W. Z. Liu. Separation and recovery of cesium sulfate from the leach solution obtained in the sulfuric acid baking process of lepidolite concentrate. *Hydrometallurgy*, Vol. 199, 2021, id. 105537.

[36] Zhang, J. F., L. G. Yang, T. T. Dong, F. Pan, H. F. Xing, and H. Z. Liu. Kinetics-controlled separation intensification for cesium and rubidium isolation from salt lake brine. *Industrial & Engineering Chemistry Research*, Vol. 57, No. 12, 2018, pp. 4399–4406.

[37] Li, Z., Y. Pranolo, Z. W. Zhu, and C. Y. Cheng. Solvent extraction of cesium and rubidium from brine solutions using 4-tert-butyl-2-(α-methylbenzyl)-phenol. *Hydrometallurgy*, Vol. 171, 2017, pp. 1–7.

[38] Huang, D. F., G. X. Ma, P. Lv, and Q. B. Zhou. Extraction of rubidium ion from brine solutions by dicyclohexano-18-crown-6/ionic liquid system. *The Polish Journal of Chemical Technology*, Vol. 25, No. 1, 2023, pp. 61–68.

[39] Liu, S. M., H. H. Liu, Y. J. Huang, and W. J. Yang. Solvent extraction of rubidium and cesium from salt lake brine with t-BAMBP-kerosene solution. *Transactions of Nonferrous Metals Society of China*, Vol. 25, No. 1, 2015, pp. 329–334.

[40] Shi, Q., H. Y. Zhang, J. X. Jiao, X. F. Sun, J. K. Sun, Y. T. Xie, et al. Poly (styrene-co-4-hydroxystyrene) nanofiber membrane for highly selective and efficient Rb^+ capture from high salinity solution. *Separation and Purification Technology*, Vol. 312, 2023, id. 123334.

[41] Sun, X. F., Y. Wang, H. Y. Zhang, Y. Shen, Q. Shi, H. H. Chen, et al. Fabrication and performance of the ammonium molybdophosphate/polysulfone mixed matrix membranes for rubidium adsorption in aqueous solution. *Journal of Applied Polymer Science*, Vol. 139, No. 11, 2022, id. 51798.

[42] Jia, Z. Q., S. Hao, X. X. Cheng, X. Y. Liu, and L. Y. Tu. Fabrication of prussian blue/polydopamine layers on polyacrylonitrile membranes for efficient adsorption of cesium. *Desalination and Water Treatment*, Vol. 163, 2019, pp. 125–132.

[43] Liu, Q. H., M. Liu, Z. Zhang, C. C. Yin, J. H. Long, M. J. Wei, et al. Covalent organic framework membranes with vertically aligned nanorods for efficient separation of rare metal ions. *Nature Communications*, Vol. 15, No. 1, 2024, id. 9221.

[44] Jia, Z. Q., X. X. Cheng, Y. X. Guo, and L. Y. Tu. In-situ preparation of iron (III) hexacyanoferrate nano-layer on polyacrylonitrile membranes for cesium adsorption from aqueous solutions. *Chemical Engineering Journal*, Vol. 325, 2017, pp. 513–520.

[45] He, J. T., L. Y. Mao, X. H. Ma, J. Y. Hua, Z. Y. Cui, B. Q. He, et al. Highly-Efficient adsorptive separation of Cs^+ from aqueous solutions by porous polyimide membrane containing dibenzo-18-crown-6. *Separation and Purification Technology*, Vol. 299, 2022, id. 121757.

[46] Zhang, X., X. D. Zheng, T. T. Xu, G. M. Li, J. F. Mei, Z. Y. Li, et al. Construction of imprinted bacterial cellulose composite membranes for selective adsorption of cesium from low concentration radioactive wastewater. *ACS Applied Nano Materials*, Vol. 7, No. 16, 2024, pp. 19233–19243.

[47] Rajec, P. and K. Domianová. Cesium exchange reaction on natural and modified clinoptilolite zeolites. *Journal of Radioanalytical and Nuclear Chemistry*, Vol. 275, No. 3, 2008, pp. 503–508.

[48] Munthali, M. W., E. Johan, H. Aono, and N. Matsue. Cs^+ and Sr^{2+} adsorption selectivity of zeolites in relation to radioactive decontamination. *Journal of Asian Ceramic Societies*, Vol. 3, No. 3, 2015, pp. 245–250.

[49] Qian, Y. L., D. Ding, K. X. Li, D. Z. Fang, Y. P. Wang, Y. Q. Hu, et al. Extraction of rubidium and cesium from a leach solution of lepidolite with biomass carbon adsorbents. *Hydrometallurgy*, Vol. 208, 2022, id. 105802.

[50] Khandaker, S., Y. Toyohara, G. C. Saha, M. R. Awual, and T. Kuba. Development of synthetic zeolites from bio-slag for cesium adsorption: kinetic, isotherm and thermodynamic studies. *Journal of Water Process Engineering*, Vol. 33, 2020, id. 101055.

[51] Ye, X. S., Z. J. Wu, W. Li, H. N. Liu, Q. Li, B. J. Qing, et al. Rubidium and cesium ion adsorption by an ammonium molybdophosphate-calcium alginate composite adsorbent. *Colloids and Surfaces A: Physicochemical and Engineering*, Vol. 342, No. 1-3, 2009, pp. 76–83.

[52] Park, Y., Y. C. Lee, W. S. Shin, and S. J. Choi. Removal of cobalt, strontium and cesium from radioactive laundry wastewater by ammonium molybdophosphate-polyacrylonitrile (AMP-PAN). *Chemical Engineering Journal*, Vol. 162, No. 2, 2010, pp. 685–695.

[53] Lian, L. S., S. Y. Zhang, N. Ma, and W. Dai. Well-designed a novel phosphomolybdic-acid@ PCN-224 composite with efficient simultaneously capture towards rubidium and cesium ions. *Polyhedron*, Vol. 207, 2021, id. 115402.

[54] Wang, Y. P., Q. Y. Zhang, K. X. Li, C. Y. Wang, D. Z. Fang, W. J. Han, et al. Efficient selective adsorption of rubidium and cesium from practical brine using a metal-organic framework-based magnetic adsorbent. *Langmuir*, Vol. 40, No. 18, 2024, pp. 9688–9701.

[55] Wang, Y. P., K. X. Li, L. Ma, D. Z. Fang, M. Liu, X. S. Ye, et al. A magnetic adsorbent with metal-organic framework based on ammonium phosphomolybdenum heteropoly tungstate (AWP): selective adsorption of Rb^+ and Cs^+ from aqueous resources and stripping with ammonium salts. *Hydrometallurgy*, Vol. 216, 2023, id. 106011.

[56] Kapnisti, M., A. G. Hatzidimitriou, F. Noli, and E. Pavlidou. Investigation of cesium uptake from aqueous solutions using new titanium phosphates ion-exchangers. *Journal of Radioanalytical and Nuclear Chemistry*, Vol. 302, No. 1, 2014, pp. 679–688.

[57] Maslova, M. V., V. I. Ivanenko, L. G. Gerasimova, and N. L. Vilkova. Study of the sorption of cesium cations by a sorbent based on titanium phosphate. Protection of Metals and Physical Chemistry of Surfaces, Vol. 55, No. 5, 2019, pp. 833–840.

[58] Wu, Y. C., J. T. Chen, Z. M. Liu, P. Na, and Z. B. Zhang. Removal of trace radioactive Cs^+ by zirconium titanium phosphate: from bench-scale to pilot-scale. *Journal of Environmental Chemical Engineering*, Vol. 10, No. 4, 2022, id. 108073.

[59] Wang, G. H., H. B. Zhang, W. L. Qian, A. Y. Tang, H. Z. Cao, W. Y. Feng, et al. Synthesis and assessment of spherogranular composite tin pyrophosphate antimonate adsorbent for selective extraction of rubidium and cesium from salt lakes. *Desalination*, Vol. 581, 2024, id. 117540.

[60] Yang, H. M., C. W. Park, I. Kim, and I. H. Yoon. Hollow flower-like titanium ferrocyanide structure for the highly efficient removal of radioactive cesium from water. *Chemical Engineering Journal*, Vol. 392, 2020, id. 123713.

[61] Li, K., C. X. Li, Y. S. Liu, J. Dong, L. L. Xu, Y. R. Li, et al. High efficiency removal of Cs^+ by Fe-Co framework PBAs from radioactive wastewater. *Journal of Environmental Chemical Engineering*, Vol. 12, No. 6, 2024, id. 114314.

[62] Yang, H. M., Y. Sihn, I. Kim, and C. W. Park. Magnetic hierarchical titanium ferrocyanide for the highly efficient and selective removal of radioactive cesium from water. *Chemosphere*, Vol. 353, 2024, id. 141570.

[63] Dong, C. C., X. C. Deng, X. Q. Guo, B. Wang, X. S. Ye, J. Fan, et al. Synthesis of potassium metal ferrocyanide/Al-MCM-41 with fast and selective adsorption of cesium. *Colloids and Surfaces A: Physicochemical and Engineering*, Vol. 613, 2021, id. 126107.

[64] Naeimi, S. and H. Faghihian. Performance of novel adsorbent prepared by magnetic metal-organic framework (MOF) modified by potassium nickel hexacyanoferrate for removal of Cs^+ from aqueous solution. *Separation and Purification Technology*, Vol. 175, 2017, pp. 255–265.

[65] Yang, N., X. Guo, J. Yu, Q. Liu, J. Y. Liu, J. H. Zhu, et al. Solar driven enhanced adsorption of radioactive Cs^+ and Sr^{2+} from nuclear wastewater by chitosan-based aerogel embedded with prussian blue analog. *Journal of Hazardous Materials*, Vol. 485, 2025, id. 136955.

[66] Lv, Y. W., B. Z. Ma, Y. B. Liu, C. Y. Wang, and Y. Q. Chen. A novel adsorbent potassium magnesium ferrocyanide for selective separation and extraction of rubidium and cesium from ultra-high salt solutions. *Journal of Water Process Engineering*, Vol. 55, 2023, id. 104225.

[67] Wu, L. H., K. Zhou, Y. C. Zheng, Y. Zeng, G. Y. Zeng, Z. Y. Cheng, et al. Efficient separation and enrichment of rubidium in salt lake brine using high-performance PAN-KCuFC-PEG adsorption composite. *Molecules*, Vol. 30, No. 6, 2025, id. 1273.

[68] Ni, J. H., B. X. Sun, P. J. Liu, and G. P. Jin. Preparation of a core-shell magnetic potassium nickel copper hexacyanoferrate/zeolitic imidazolate framework composite for rubidium adsorption. *Journal of Solid State Chemistry*, Vol. 331, 2024, id. 124554.

[69] Fang, M., W. F. Chu, J. S. Cui, G. P. Jin, and C. Q. Tian. Adsorption application of Rb^+ on hydrogels of hydroxypropyl cellulose/polyvinyl alcohol/reduced graphene oxide encapsulating potassium cobalt hexacyanoferrate. *Applied Organometallic Chemistry*, Vol. 36, No. 10, 2022, id. e6827.

[70] Jiang, C. Y., J. H. Ni, and G. P. Jin. Magnetic potassium cobalt hexacyanoferrate nanocomposites for efficient adsorption of rubidium in solution. *Separation and Purification Technology*, Vol. 296, 2022, id. 121383.

[71] Chu, W. F., Z. Z. Yuan, P. H. Lin, and G. P. Jin. Recovery of rubidium using hydrogel beads encapsulating potassium copper hexacyanoferrate from saline lake brines. *Industrial & Engineering Chemistry Research*, Vol. 63, No. 4, 2024, pp. 1988–1999.

[72] Truong, D. Q., Y. Choo, N. Akther, S. Roobavannan, A. Norouzi, V. Gupta, et al. Selective rubidium recovery from seawater with metal-organic framework incorporated potassium cobalt hexacyanoferrate nanomaterial. *Chemical Engineering Journal*, Vol. 454, 2023, id. 140107.

[73] Lee, Y. S., H. M. Yang, Y. Jeong, and G. E. Lee. Inkjet-based facile fabrication of a copper ferrocyanide-embedded magnetic alginate microadsorbent for highly enhanced cesium removal. *Carbohydrate Polymers*, Vol. 348, 2025, id. 122877.

[74] Yang, X. B., W. Li, Z. Z. Lin, J. Q. Liu, H. X. Jiang, H. Jia, et al. Ultralight, robust, and high prussian blue-loading polyacrylonitrile aerogel: preparation, characterization and efficient adsorption/removal of Cs^+. *Chemical Engineering Journal*, Vol. 464, 2023, id. 142723.

[75] Li, T. T., F. He, and Y. D. Dai. Prussian blue analog caged in chitosan surface-decorated carbon nanotubes for removal cesium and strontium. *Journal of Radioanalytical and Nuclear Chemistry*, Vol. 310, No. 3, 2016, pp. 1139–1145.

[76] Clearfield, A., L. N. Bortun, and A. I. Bortun. Alkali metal ion exchange by the framework titanium silicate $M_2Ti_2O_3SiO_4{\cdot}nH_2O$ (M = H, Na). *Reactive & Functional Polymers*, Vol. 43, No. 1–2, 2000, pp. 85–95.

[77] Liu, H. M., A. Yonezawa, K. Kumagai, M. Sano, and T. Miyake. Cs and Sr removal over highly effective adsorbents ETS-1 and ETS-2. *Journal of Materials Chemistry A: Materials for Energy and Sustainability*, Vol. 3, No. 4, 2015, pp. 1562–1568.

[78] Perovskiy, I. A., D. A. Shushkov, A. Ponaryadov, T. L. Panikorovskii, and P. Krivoshapkin. Controlled reprocessing of leucoxene concentrate for environmental friendly production of titanosilicate – an effective sorbent for strontium and cesium ions. *Journal of Environmental Chemical Engineering*, Vol. 11, No. 5, 2023, id. 110691.

[79] Eom, H. H., H. Kim, D. Harbottle, and J. W. Lee. Selective removal of Cs^+ and Sr^{2+} by electrosorption using intercalating titanosilicate. *Separation and Purification Technology*, Vol. 330, 2024, id. 125550.
[80] Liu, T., L. Miao, F. Y. Yao, W. X. Zhang, W. X. Zhao, D. S. Yang, et al. Structure, properties, preparation, and application of layered titanates. *Inorganic Chemistry*, Vol. 63, No. 1, 2024, pp. 1–26.
[81] Ide, Y., M. Sadakane, T. Sano, and M. Ogawa. Functionalization of layered titanates. *Journal of Nanoscience and Nanotechnology*, Vol. 14, No. 3, 2014, pp. 2135–2147.
[82] Liu, G., H. Y. Mei, X. L. Tan, H. F. Zhang, H. N. Liu, M. Fang, et al. Enhancement of Rb^+ and Cs^+ removal in 3D carbon aerogel-supported $Na_2Ti_3O_7$. *Journal of Molecular Liquids*, Vol. 262, 2018, pp. 476–483.
[83] Li, K. X., D. Ding, Z. Fang, Y. P. Wang, X. S. Ye, H. N. Liu, et al. Hydrothermal deposition of titanate on biomass carbonaceous aerogel to prepare novel biomass adsorbents for Rb^+ and Cs^+. *Colloids and Surfaces A: Physicochemical and Engineering*, Vol. 590, 2020, id. 124501.
[84] Amesh, P., K. A. Venkatesan, A. S. Suneesh, and U. Maheswari. Tuning the ion exchange behavior of cesium and strontium on sodium iron titanate. *Separation and Purification Technology*, Vol. 267, 2021, id. 118678.
[85] Geng, W. L., D. B. Wang, Y. F. Liu, J. L. Zhang, L. M. Zhong, R. X. Lin, et al. Preparation of layered titanate nanosheets and the application for Cs^+ adsorption from wastewater, effluents and a simulated brine. *Hydrometallurgy*, Vol. 216, 2023, id. 105999.
[86] Geng, W. L., Y. F. Liu, D. B. Wang, M. Y. Lin, X. Yang, L. M. Zhong, et al. $H_2Ti_6O_{13}$ nanosheet/polymethyl methacrylate (PMMA) for the adsorption of cesium ions. *Journal of Solid State Chemistry*, Vol. 324, 2023, id. 124047.
[87] Yang, X., M. Lin, J. M. Chu, and D. Q. Dong. Preparation of highly hydrophilic cesium ion sieve and its performance in adsorbing Cs^+. *Chemical Physics*, Vol. 588, 2025, id. 112438.
[88] Chitrakar, R., Y. Makita, and A. Sonoda. Cesium adsorption by synthetic todorokite-type manganese oxides. *Bulletin of the Chemical Society of Japan*, Vol. 87, No. 6, 2014, pp. 733–739.
[89] Liu, Z., Y. Q. Zhou, M. Guo, B. L. Lv, Z. J. Wu, and W. Z. Zhou. Experimental and theoretical investigations of Cs^+ adsorption on crown ethers modified magnetic adsorbent. *Journal of Hazardous Materials*, Vol. 371, 2019, pp. 712–720.
[90] Chen, X., Y. Wang, B. X. Liu, L. Gao, L. L. Qiao, C. W. Xiong, et al. Ecologically friendly 2D/2D Na^+-MXene/LDH for cesium adsorption in salt lakes: a comprehensive study on adsorption performance, mecnisms, and environmental impact. *Desalination*, Vol. 602, 2025, id. 118632.
[91] Xu, Z. H., M. Rong, S. Ni, Q. Y. Meng, X. Wu, H. Z. Liu, et al. Self-polycondensing hypercross-linked polymers from hydroxybenzyl alcohols for efficient cesium adsorption. *ACS Applied Polymer Materials*, Vol. 5, No. 10, 2023, pp. 8315–8325.